A PRECISE MEASUREMENT OF b BARYON LIFETIME

by

YONGSHENG GAO

A dissertation submitted in partial fulfillment

of the requirements for the degree of

Doctor of Philosophy

(Physics)

at the

UNIVERSITY OF WISCONSIN-MADISON

1995

A PRECISE MEASUREMENT OF b BARYON LIFETIME

Yongsheng Gao

Under the supervision of Professor Sau Lan Wu

at the University of Wisconsin-Madison

ABSTRACT

In about 1,500,000 hadronic Z decays recorded with the ALEPH detector in 1991, 1992 and 1993, the yields of $\Lambda\ell^{\perp}$ combinations are measured. Semileptonic decays of b baryons result in a signal of $290 \pm 35(\mathrm{stat}) \pm 39(\mathrm{syst})$ $\Lambda\ell^{\perp}$ combinations from b baryon decays, which corresponds to a product branching ratio:

$$\mathrm{Br}(\mathrm{b} \to \Lambda_\mathrm{b}) \cdot \mathrm{Br}(\Lambda_\mathrm{b} \to \Lambda_\mathrm{c}^+ \ell^{\perp} \overline{\nu} X) \cdot \mathrm{Br}(\Lambda_\mathrm{c}^+ \to \Lambda X)$$

$$= (0.61 \pm 0.07(\mathrm{stat}) \pm 0.10(\mathrm{syst}))\%$$

From a maximum likelihood fit to the impact parameter distribution of leptons in 519 $\Lambda\ell^{\perp}$ combinations containing a b baryon sample of 290 decays, the measured b baryon lifetime is:

$$\tau_{\Lambda_\mathrm{b}} = 1.05^{+0.12}_{\perp 0.11}(\mathrm{stat}) \pm 0.09(\mathrm{syst}) \text{ ps}$$

Comparing with the current b meson lifetime measurements, the b baryon lifetime is found to be substantially smaller than b meson lifetimes.

Acknowledgements

This thesis is really the result of many people's efforts. I would like to take this opportunity to thank the many people who have contributed, directly or indirectly, to this thesis.

I would like to thank my advisor, Prof. Sau Lan Wu, who has guided and supported me throughout my entire graduate studies for high energy physics. Her dedication to and enthusiasm for physics are extremely inspiring. Her insight into physics and her persistence in the pursuit of the beauty of physics have been an example to me all the time. I benefitted greatly also from the first-class physics and computational environments she has provided the Wisconsin group which made the research work in the group very fruitful.

I owe Dr. Vivek Sharma a great deal in his expert help and guidance for the analysis presented in this thesis. I benefitted greatly from his valuable suggestions and comments and appreciated more and more the beauty and simplicity of physics by working with him. It is always educational and pleasant to discuss with him. I really enjoyed the times we spent in the CERN cafeteria discussing the possible solutions to physics problems we encountered and the feasibilities of different new ideas, with a PDG booklet, a pen, some scratch paper and a beer.

The analysis presented in this thesis was done between 1993 and 1994 in collaboration with Dr. Lorenzo Moneta who is now at Imperial College, London. His experience in impact parameter analysis and understanding of physics as well as his nice personality were very impressive and made our collaboration very pleasant and fruitful.

I am indebted to Dr. Ian Scott, Dr. Michael Schmitt, Dr. Joleen Pater, Dr. Fred Weber, Dr. Leo Bellantoni, Dr. YiBin Pan and Dr. HongBo Hu for inspiring discussions throughout my research work in the Wisconsin group at CERN. Vivek, Ian and Michael also read the draft of this thesis and gave valuable suggestions. I would also like to thank Dr. Michael Wash, Doug Ferguson and Owen Hayes who kindly read over this thesis and corrected numerous errors concerning the grammar and spelling.

Ms HuiZhen Gao made a number of beautiful plots for this thesis. I am very grateful to her for her patience and the beautiful work she did when she was extremly busy with her own work.

Sloan Looney did a great deal of Monte Carlo generation for this analysis and he also did an excellent job together with Chris Lishka and Dr. Haimo Zobernig in maintaining the smooth running of the Wisconsin computers which has been essential for the high productivity of the Wisconsin group.

I benefited a lot from valuable discussions with many people in the ALEPH Collaboration. Among them are Prof. Luigi Rolandi, Prof. Jacques LeFrançois, Prof. Wolf-Dieter Schlatter, Prof. Alan Litke and Dr. Roger Forty.

I am lucky to have friends like YiBin, HongBo, Dr. Zhong Feng, Min Zheng, XiDong Wu, XiaoYing Cui, HanGue Wang and WeiHua Tian who have made my life very colorful during my stay at CERN. It's always a pleasure to play tennis with Arthur Secret, Dr. Jeff Turk, Tom Greening and XiDong. I would like to thank Dr. Ian Brock, Rosi Wilde-Brock, Merlene Tanke, Mathias Beck, Nicole Gonthier together with other members in the badminton club of Satigny. The trophies I won in the men's doubles and mixed doubles at the "Championnat Genevois de Badminton" in 1993 and 1994 with Mathias and Angele Rutz will always remind me of their hospitality, friendship and care.

Dr. Hang Deng can never be thanked enough. I will always be grateful to her for her understanding, support, and more importantly, her inspiration in many aspects.

Finally I would like to thank my parents ZhenSheng Gao and MianMian Zhou for their love, emotional support and encouragement they gave me, throughout my graduate studies in the the United States. They were the first who introduced the basic idea of science to me and they supported me throughout my whole education in China and eventually made my trip to the United States for my Ph.D studies possible. I would also like to thank them for their understanding and toleration of my absence.

Contents

Chapter 1

Introduction

1.1 Motivation

Since the discovery of the b quark in 1977 [1], much information has been collected about b hadrons. In the early 80's, measurements of the average b hadron lifetime at PEP and PETRA [2] provided the first estimate of the magnitude of the Cabibbo-Kobayashi-Maskawa (CKM) matrix [3] element $V_{\rm cb}$ and contradicted with the phenomenological expectations prevalent at that time. Measurements of individual b hadron lifetimes are of interest because they test the present understanding of b hadron decay dynamics. In the simple "Spectator Model" picture [4], the light quarks in the hadron (called the spectator quarks) are not expected to play a big role in the decay of the hadron, and hence the lifetimes of the various b hadron species are equal. As is well known, the Spectator Model does not work well in the charm system where large differences are seen between the different charm hadron lifetimes [5]:

$$\tau(D^{\pm}) \simeq 2.5\tau(D^0) \simeq 2.3\tau(D_s^{\pm}) \simeq 5.3\tau(\Lambda_c^{\pm})$$

In order to explain the hierarchy in charm hadron lifetimes, many alternative non-spectator effects such as W-exchange or W-annihilation and improved versions of the Spectator Model incorporating the corrections due to non-perturbative QCD corrections have been considered [6]. Non-spectator effects are expected to be small in the case of b mesons, but could be larger in the b baryon decays due to the lack of helicity suppression. In contrast to the diversity observed in the lifetimes of charm hadrons, the differences among various b hadron species are expected to be not too much larger than 10% [7], due to the larger b quark mass. Measurements at LEP [8] and the Tevatron [9] have confirmed the expected equality of the b mesons lifetimes, but the published measurements [10] of b baryon lifetime have not yet reached the necessary precision for an interesting comparison of b meson and b baryon lifetimes. This dissertation presents a precise measurement of the b baryon lifetime using a data sample of about 1,500,000 hadronic Z decays recorded with the ALEPH detector in 1991, 1992 and 1993.

The remainder of this chapter gives a brief introduction of the concepts relevant to the b baryon lifetime measurement. Chapter 2 gives a brief description of the LEP collider, the ALEPH detector, together with the event reconstruction and particle identification in ALEPH. Chapter 3 and 4 respectively present the isolation of b baryon signal and the measurement of b baryon lifetime. Chapter 5 gives the conclusion, a summary of the current b hadron lifetime measurements and a future

Quarks			Leptons		
Symbol	Charge	Mass	Symbol	Charge	Mass
up(u)	+2/3	2-8	ν_e	0	< 0.005
down(d)	-1/3	5-15	e	-1	0.511
charm(c)	+2/3	1000-1600	ν_μ	0	< 0.27
strange(s)	-1/3	100-300	μ	-1	105.66
top(t)	+2/3	174000	ν_τ	0	< 31
bottom(b)	-1/3	4100-4500	τ	-1	1777.1

Table 1.1: Fundamental fermions of particle physics. Only the particles are shown, the corresponding antiparticles are denoted with a bar over the symbol and have the same mass but the opposite charge as the particle. All masses are given in MeV/c^2.

outlook.

1.2 The Fundamental Particles and Interactions

According to our current understanding, matter is composed of fundamental spin 1/2 particles which are divided into two groups, quarks and leptons. Table 1.1 lists the charges and masses of the quarks and leptons.

Leptons can exist as free particles, while quarks are bound into hadrons, either as a quark-antiquark pair forming a meson or as three quarks forming a baryon. The b, c and t quarks are referred to as “heavy" flavors, while the u, d and s are called “light" quarks.

There are four fundamental interactions: electromagnetic, strong, weak and gravitational. The effect of gravitation upon the processes relevant to the work presented here is extremely small and will not be discussed here.

Force	Mediator	Charge	Mass	Spin
Strong	gluon(g)	0	0	1
Electromagnetic	photon(γ)	0	0	1
Weak	$W^{\pm}$, Z	$\pm$1,0	80,91	1

Table 1.2: Fundamental forces and their mediators. Masses are in GeV/c^2.

The electromagnetic, strong and weak forces are mediated by the exchange of gauge bosons whose properties are listed in Table 1.2.

As established in the 60's and 70's [11], the electromagnetic and weak forces can be considered as two aspects of a single, more fundamental electroweak interaction. This interaction is described by a gauge theory incorporating a SU(2) symmetry of weak isospin and an U(1) symmetry of weak hypercharge. This symmetry is spontaneously broken by the Higgs mechanism [12], which generates masses for the quarks and leptons and gives rise to the massive $W^{\pm}$ and Z bosons, the massless photon, and a massive scalar boson H^0, the Higgs particle. This theory is referred to as the “Standard Model" of electroweak interactions. The Standard Model has been remarkably successful in describing the observed physical phenomena, and in making predictions that have later been verified experimentally, such as the existence of the charm quark [13], the $W^{\pm}$ [14] and Z [15] bosons.

In the Standard Electroweak Model, fermions interact via the exchange of a W^{+} or $W^{\perp}$ boson (the “charged-current interaction") or by the exchange of a Z boson or a γ (the “neutral-current interaction"). In the limit of massless fermions, the $W^{\pm}$ only couple to left-handed fermions (and right-handed antifermions). The left-handed quarks and leptons can be arranged in weak isospin doublets, while the right-handed fermions are isospin singlets:

$$\begin{pmatrix} \mathrm{u} \\ \mathrm{d}' \end{pmatrix}_{\mathrm{L}}, \begin{pmatrix} \mathrm{c} \\ \mathrm{s}' \end{pmatrix}_{\mathrm{L}}, \begin{pmatrix} \mathrm{t} \\ \mathrm{b}' \end{pmatrix}_{\mathrm{L}}, \begin{pmatrix} \nu_e \\ e^{\perp} \end{pmatrix}_{\mathrm{L}}, \begin{pmatrix} \nu_\mu \\ \mu^{\perp} \end{pmatrix}_{\mathrm{L}}, \begin{pmatrix} \nu_\tau \\ \tau \end{pmatrix}_{\mathrm{L}},$$

$$\mathrm{u_R},\ \mathrm{d_R},\ \mathrm{c_R},\ \mathrm{s_R},\ \mathrm{b_R},\ \mathrm{t_R}$$

$$e_{\mathrm{R}},\ \mu_{\mathrm{R}},\ \tau_{\mathrm{R}}$$

The weak eigenstates d', s' and b' are related to the mass eigenstates d, s and b by a unitary rotation matrix called the Cabibbo-Kobayashi-Maskawa (CKM) matrix [3]:

$$\begin{pmatrix} \mathrm{d}' \\ \mathrm{s}' \\ \mathrm{b}' \end{pmatrix} = \begin{pmatrix} V_{\mathrm{ud}} & V_{\mathrm{us}} & V_{\mathrm{ub}} \\ V_{\mathrm{cd}} & V_{\mathrm{cs}} & V_{\mathrm{cb}} \\ V_{\mathrm{td}} & V_{\mathrm{ts}} & V_{\mathrm{tb}} \end{pmatrix} \begin{pmatrix} \mathrm{d} \\ \mathrm{s} \\ \mathrm{b} \end{pmatrix} \tag{1.1}$$

The values of the elements of CKM-matrix are determined by experiments as follows [5]:

$$\begin{pmatrix} V_{\mathrm{ud}} & V_{\mathrm{us}} & V_{\mathrm{ub}} \\ V_{\mathrm{cd}} & V_{\mathrm{cs}} & V_{\mathrm{cb}} \\ V_{\mathrm{td}} & V_{\mathrm{ts}} & V_{\mathrm{tb}} \end{pmatrix} = \begin{pmatrix} .9747 \text{ to } .9759 & .218 \text{ to } .224 & .002 \text{ to } .005 \\ .218 \text{ to } .224 & .9738 \text{ to } .9752 & .032 \text{ to } .048 \\ .004 \text{ to } .015 & .030 \text{ to } .048 & .9988 \text{ to } .9995 \end{pmatrix} \tag{1.2}$$

The strong interaction is described by a gauge group based on a SU(3)$_C$ symmetry of color, called Quantum Chromodynamics (QCD). The mediators of the strong interaction are eight massless gluons which have spin 1 and carry a quantum number called color. Quarks are the only fundamental fermions that carry color. The coupling of the strong force increases with particle separation. This forces all stable matter to be colorless, preventing the existence of free quarks. This is referred to as “confinement".

1.3 b Hadron Production in Z Decays and Quark Fragmentation

1.3.1 b Hadron Production in Z Decays

The production of fermion pairs ($\mathrm{f\bar{f}}$) in $e^+e^\perp$ collisions is pictured in Figure 1.1. The incoming electron and positron annihilate via weak neutral current to form a fermion-antifermion pair. As LEP operates at or near the peak of the Z resonance, the relative contribution from the photon-exchange diagram is negligible. All $\mathrm{f\bar{f}}$, except $\mathrm{t\bar{t}}$ which is too heavy, can be produced in Z decays. Since in each case $m_\mathrm{f} \ll m_\mathrm{Z}$, the fermions can be assumed to be massless. The partial width for the decay of a Z to fermions within the Standard Model is then given by:

$$\Gamma(\mathrm{Z} \rightarrow \mathrm{f\bar{f}}) = \frac{G_\mathrm{F} M_\mathrm{Z}^3}{6\pi\sqrt{2}} C((g_\mathrm{V}^\mathrm{f})^2 + ((g_\mathrm{A}^\mathrm{f})^2) \quad (1.3)$$

where G_F is the Fermi coupling constant, M_Z is the mass of the Z boson, C is the color factor of the fermion (1 for leptons, 3 for quarks) and g_V^f and g_A^f are the

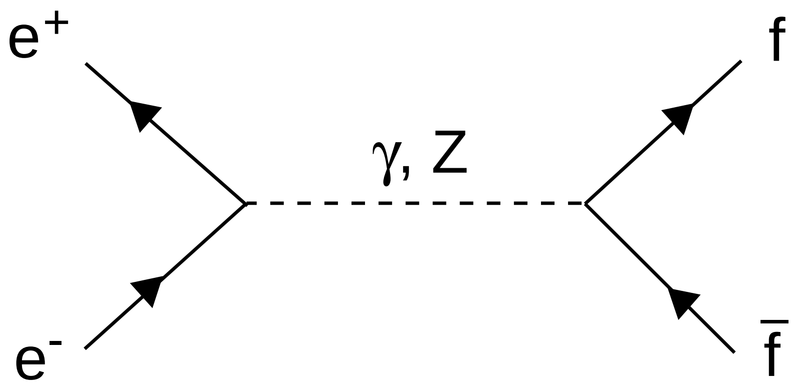

Figure 1.1: Feynman diagram depicting the annihilation of an electron with a positron to form either a Z boson or a photon, which subsequently decays into a fermion-antifermion pair.

vector and axial-vector couplings of the Z to the fermions. In the Standard Model these couplings are given by:

$$g_{\mathrm{V}}^{\mathrm{f}} = I_3^{\mathrm{f}} \perp 2q^{\mathrm{f}} \sin^2\theta_{\mathrm{W}}(M_{\mathrm{Z}}^2) \quad (1.4)$$

$$g_{\mathrm{A}}^{\mathrm{f}} = I_3^{\mathrm{f}} \quad (1.5)$$

where q^{f} is the fermion's charge, $\theta_{\mathrm{W}}(M_Z^2)$ is the electroweak mixing angle at the Z mass, and I_3^{f} is the third component of the weak isospin of the fermion.

The total width Γ of any particle is the sum of its partial decay widths, and is related to its lifetime by $\Gamma = \frac{1}{\tau}$.

The electroweak parameters measured at LEP are [16]:

$$M_{\mathrm{Z}} = 91.1887 \pm 0.0022\mathrm{GeV}$$

$$\sin^2\theta_{\mathrm{W}} = 0.2320 \pm 0.0016$$

$$\Gamma(\mathrm{Z} \to \mathrm{all}) = 2.4971 \pm 0.0031 \pm 0.0010\mathrm{GeV}$$

$$\Gamma(\mathrm{Z} \to \mathrm{hadron}) = 1.7460 \pm 0.0031\mathrm{GeV}$$

$$\mathrm{R_b} = \frac{\Gamma(\mathrm{Z} \to \mathrm{b\bar{b}})}{\Gamma(\mathrm{Z} \to \mathrm{hadron})} = 0.2204 \pm 0.0020$$

1.3.2 Quark Fragmentation

The Z $\to \mathrm{q\bar{q}}$ decay produces a back-to-back quark-antiquark pair. However, color confinement requires that only color singlet hadrons can exist in the final state. This process is known as “hadronization" or “fragmentation" which cannot be calculated exactly and is only phenomenologically understood. One parameterization of fragmentation is based on a string-breaking model [17]. As the quark and antiquark separate, the energy stored in the string rises with the separation between the q and $\mathrm{\bar{q}}$. At some point, the stored energy in the string is larger than the energy required to create a $\mathrm{q\bar{q}}$ from the vacuum, and the string breaks into two pieces. This process repeats until the energy in the string falls below a cutoff.

A quark q and antiquark $\mathrm{\bar{q}}$ are most likely to combine into a meson when they have about the same velocity. If the fragmenting parton is a heavy quark Q, it needs to lose only a small fraction of its energy in order to materialize a number of light quark pairs with comparable velocity. If Q then combines with one or more of these light quarks, the resulting heavy-flavored hadron H_Q with energy E_H will carry a large fraction of the original energy: $z = E_H/E_Q \sim 1$; while for light quarks, $z \ll 1$. We therefore expect qualitatively that the fragmentation of heavy quarks into heavy hadrons will have a hard distribution, concentrated at large values of z, and that this property will become more marked as the quark mass increases. A successful example of such a parameterization is the fragmentation function derived by Peterson et al. [18]:

$$f(z) = \frac{1}{z[1 \perp (1/z) \perp \epsilon_Q/(1 \perp z)]^2}$$

where ϵ_Q is a constant, different for each quark flavor. For Q = c and b with $\epsilon_c = 0.15$ and $\epsilon_b = (m_c/m_b)^2\epsilon_c$. The high momentum fragmentation particles distinguish heavy quark fragmentation from light quark fragmentation (Figure 1.2).

It is apparent that in the meson case, only one pair of quarks is needed from the vacuum, while in the baryon case, two pairs are needed. This makes the production, and hence the observation of baryons more difficult than mesons. To find a way of overcoming this difficulty and obtaining a clear and convincing signature of the b baryon is one of the tasks of this dissertation.

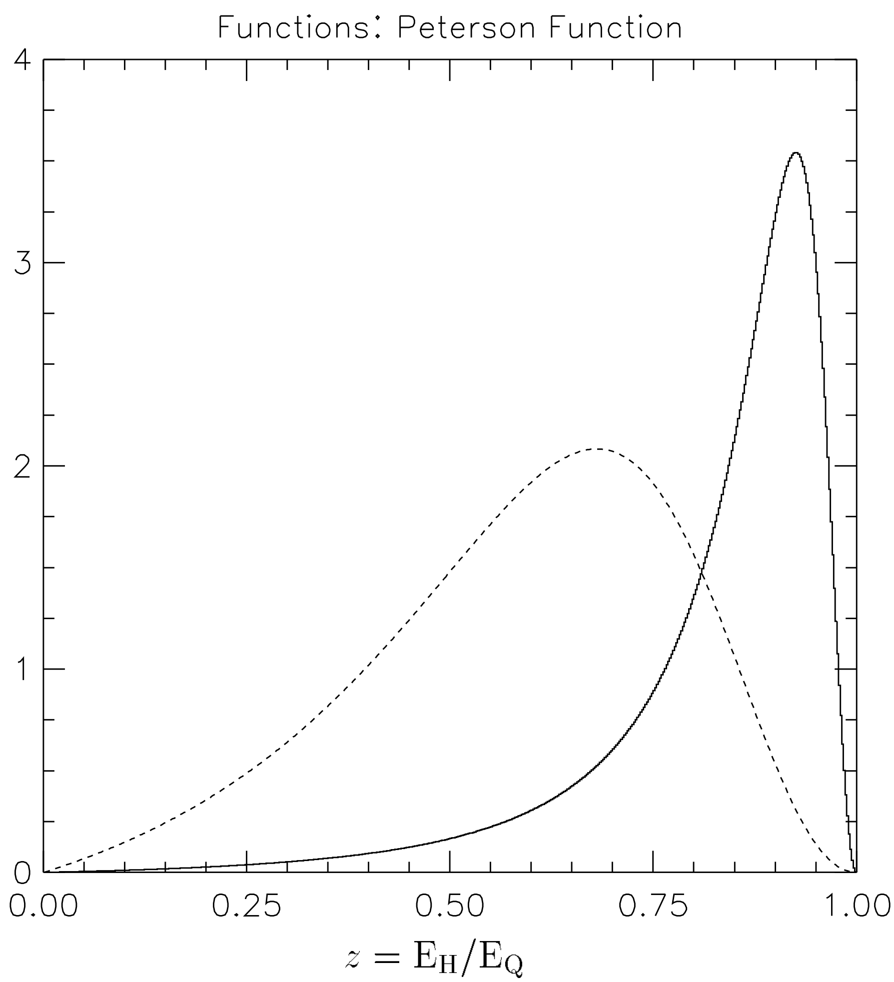

Figure 1.2: Fragmentation functions for b quark (solid line) and c quark (dashed line).

1.4 b Baryon Decay and Lifetime Measurement

The simplest model describing the decay of a hadron containing a heavy quark is the Spectator Model [4]. In this model, the heavy quark decays via the weak charged current (i.e. by the emission of a virtual W^{+} or $W^{\perp}$ boson) to a lighter quark. The additional quark (in the meson case) or diquark (in the baryon case) in the hadron acts simply as a spectator (Figure 1.3(a)).

The semileptonic widths of the D^0 and the $D^{\pm}$ have been measured to be approximately equal, so the Spectator Model can be taken as a reasonable approximation for semileptonic decays. If the light quark has no influence on the decay of the hadron as described by the Spectator Model, the decay widths and therefore the lifetimes of all hadrons containing a given heavy quark would be identical in this model. It has been shown experimentally [5] that in the system of c hadrons:

$$\tau(D^0) = 4.15 \pm 0.04 \times 10^{\perp 13}\mathrm{s}$$

$$\tau(D^{\pm}) = 10.57 \pm 0.15 \times 10^{\perp 13}\mathrm{s}$$

$$\tau(D_{\mathrm{s}}^{\pm}) = 4.67 \pm 0.17 \times 10^{\perp 13}\mathrm{s}$$

$$\tau(\Lambda_{\mathrm{c}}^{\pm}) = 2.00 \pm 0.11 \times 10^{\perp 13}\mathrm{s}$$

The differences in the lifetimes of the c hadron system indicate that there may be other processes that contribute to the decays of hadrons containing heavy quark. To explain the scale of these differences, several possible processes have been suggested that go beyond the simple Spectator Model:

- W annihilation (Figure 1.3 (b)).
- Internal W conversion (Figure 1.3 (c)).
- W exchange (Figure 1.3 (d)).

Hence it is important to consider whether these non-spectator amplitudes can also result in significant lifetime differences in the b system.

The "W annihilation" (Figure 1.3 (b)) affects the decays of charged b mesons only, and it is negligible in B^+ decays because of the smallness of the CKM matrix element $V_{\rm ub}$. In the "Internal W conversion", shown in Figure 1.3 (c), the quarks from the virtual W are shared between the daughter quark and the spectator. This can only happen when the colors of the initial heavy quark and the quarks from the W are the same. Thus, this process is called a "color suppressed" process. Naively, the color matching probability is 1/3 in the amplitude, so color suppressed decays should occur about 1/9 of the time. The size of this effect has been estimated to be less than 1% [19], or as much as a few percent [20]. The "W exchange" (Figure 1.3 (d)) affects only the decays of neutral b hadrons. The effect is small in b meson decays due to helicity suppression, but could be larger in b baryon decay case due to the lack of helicity suppression. In contrast to the diversity observed in the lifetimes of charm hadrons, the differences among various b hadron species

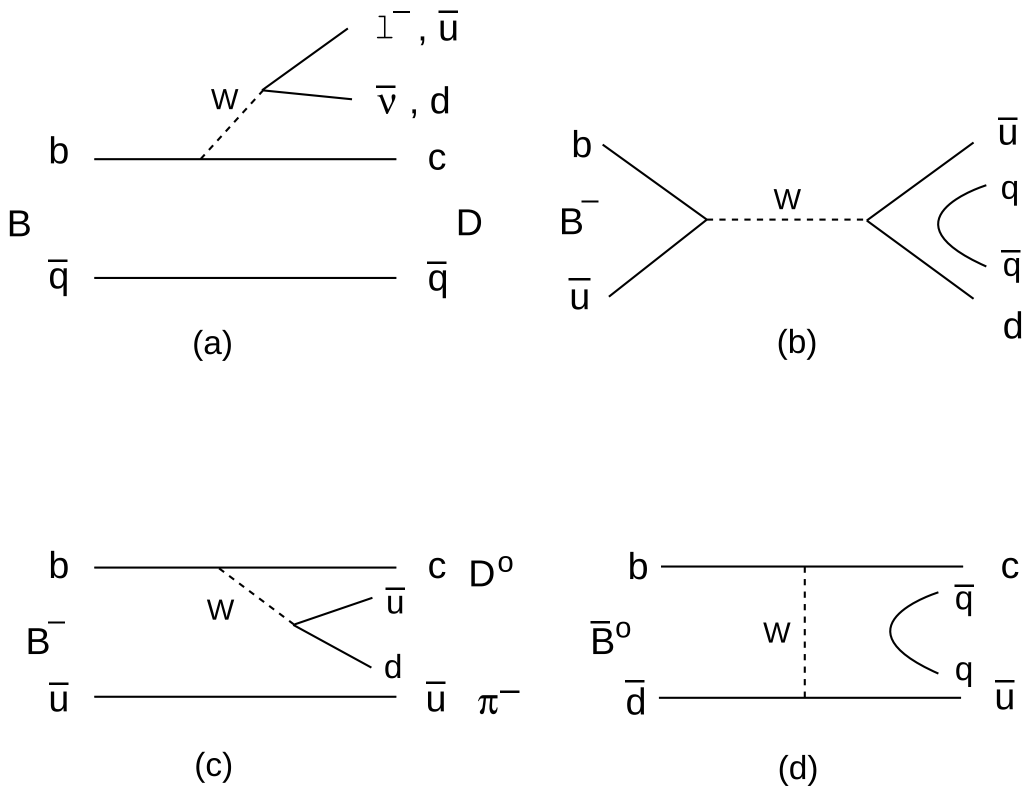

Figure 1.3: Spectator and Non-Spectator decay diagrams for B mesons. (a) is the spectator decay diagram, (b) is the W annihilation diagram, (c) is the internal W conversiona diagram and (d) is the W exchange diagram.

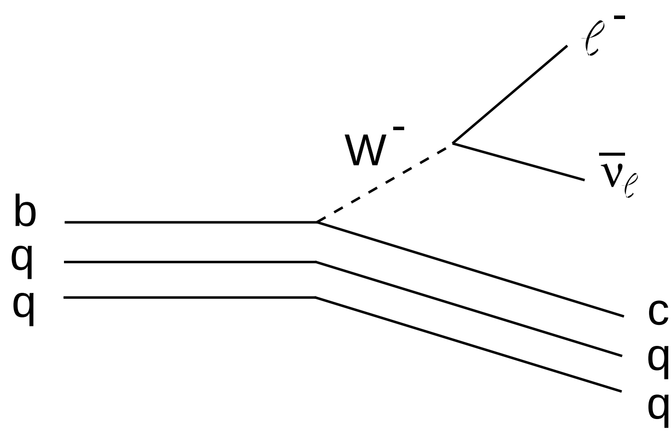

Figure 1.4: Diagram of semileptonic b baryon decay.

are expected to be not much larger than 10% [7]. However, it is difficult to make a specific prediction for the contribution of these non-spectator effects in the b baryon case. More precise measurements of b hadron lifetimes, especially the b baryon lifetime are needed to understand the dynamics of b hadron decay.

Semileptonic decays (Figure 1.4) play a prominent role in heavy quark physics. There are several reasons for this. First, these decays are the simplest to understand theoretically. They proceed via the spectator diagram. Models must account for strong interaction effects only among less quarks (b, diquark and c or u) than in the more complicated case of hadronic decay. Second, the charge of the lepton indicates the flavor of the b-hadron at the time of its decay. A negative charge shows that the hadron contained a b-quark while a positive charge indicates a $\bar{b}$ quark. Third, the branching ratios are large in b hadron decays, allowing for thorough experimental study.

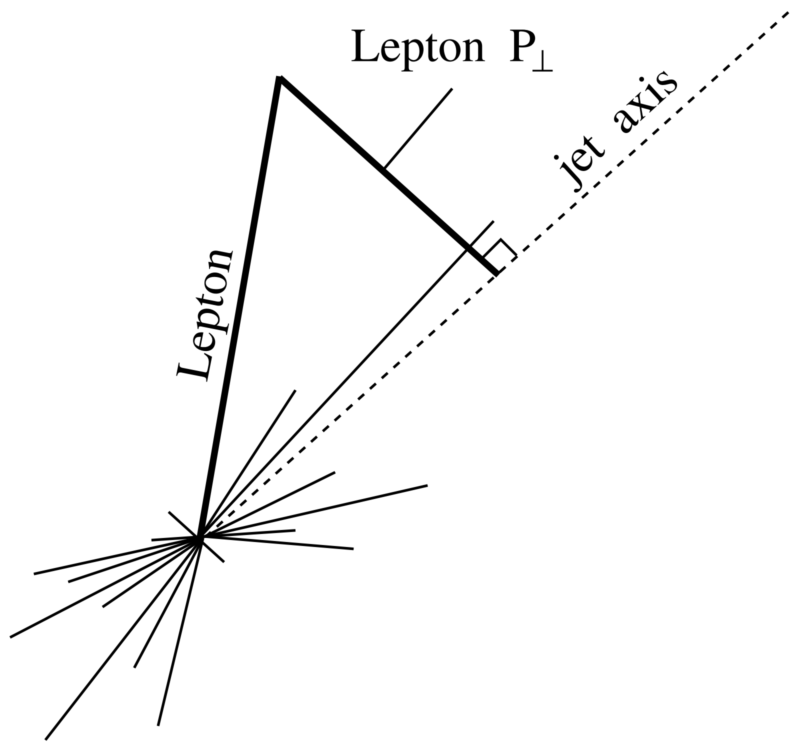

Figure 1.5: Definition of the transverse momentum of a track in a jet.

The semileptonic b-hadron decays are studied using the fact that the b-quarks are the heaviest quarks produced at $\sqrt{s} = M_Z$. The large mass of the b-quark leads to decay products with, on average, higher transverse momentum with respect to the jet axis than the particles in jets from lighter quarks. Let $P_\perp$ denote the momentum of a lepton perpendicular to the jet with which the lepton is associated (Figure 1.5). The leptons from semileptonic b hadron decays will have higher transverse momenta $P_\perp$ than the leptons from the decay of lighter flavored hadrons.

Also, as mentioned in the discussion of fragmentation, the b-hadron decays have the hardest fragmentation. Consequently their leptonic decay products will have, on average, higher lab-frame momenta than the leptons associated with the hadrons formed from lighter quarks.

Figure 1.6 compares the $P_{\perp}$ distribution for the leptons from b decays and from the other quark decays. From the plot, we can easily see that the requirement of higher lepton $P_{\perp}$ is good tagging method to sort out b decays.

Evidence for b baryons in Z decays via correlation between a Λ and a high transverse momentum prompt lepton has been reported previously by the ALEPH [21], OPAL [22] and DELPHI [23] collaborations. The signal results from the decay[1] $\Lambda_{\mathrm{b}} \to \Lambda_{\mathrm{c}}^{+}\ell^{\perp}\overline{\nu}$ followed by the decay $\Lambda_{\mathrm{c}}^{+} \to \Lambda X$, with the Λ decaying to p$\pi^{\perp}$. The correlation $\Lambda\ell^{\perp}$, as opposed to $\Lambda\ell^{+}$, is a distinctive signature of semileptonic b baryon decay, with weak decays of the Λ_{b} expected to dominate the b baryon sample [24, 25]. Λ_{b} is a generic name for b baryons throughout this dissertation. Evidence for semileptonic b baryon decays and lifetime measurement of Λ_{b} with the exclusive reconstruction of the Λ_{c}^{+} i.e. $\Lambda_{\mathrm{b}} \to \Lambda_{\mathrm{c}}^{+}\ell^{\perp}\overline{\nu}$ where $\Lambda_{\mathrm{c}}^{+} \to \mathrm{pK}^{\perp}\pi^{+}$, have also been reported by ALEPH [26, 27], though with poor precision.

In general, in the decay $\Lambda_{\mathrm{b}} \to \Lambda_{\mathrm{c}}^{+}\ell^{\perp}\overline{\nu}$ followed by $\Lambda_{\mathrm{c}}^{+} \to \Lambda X$, not all the decay products of the c baryon can be reconstructed. Furthermore, as the Λ decays far away from the primary vertex, it provides little information about the c baryon decay vertex. Nevertheless the decay $\Lambda_{\mathrm{c}}^{+} \to \Lambda X$ has a large branching ratio and yields a much larger b baryon sample than in the the case of exclusive

[1] Charge conjugate decays are implied throughout this dissertation.

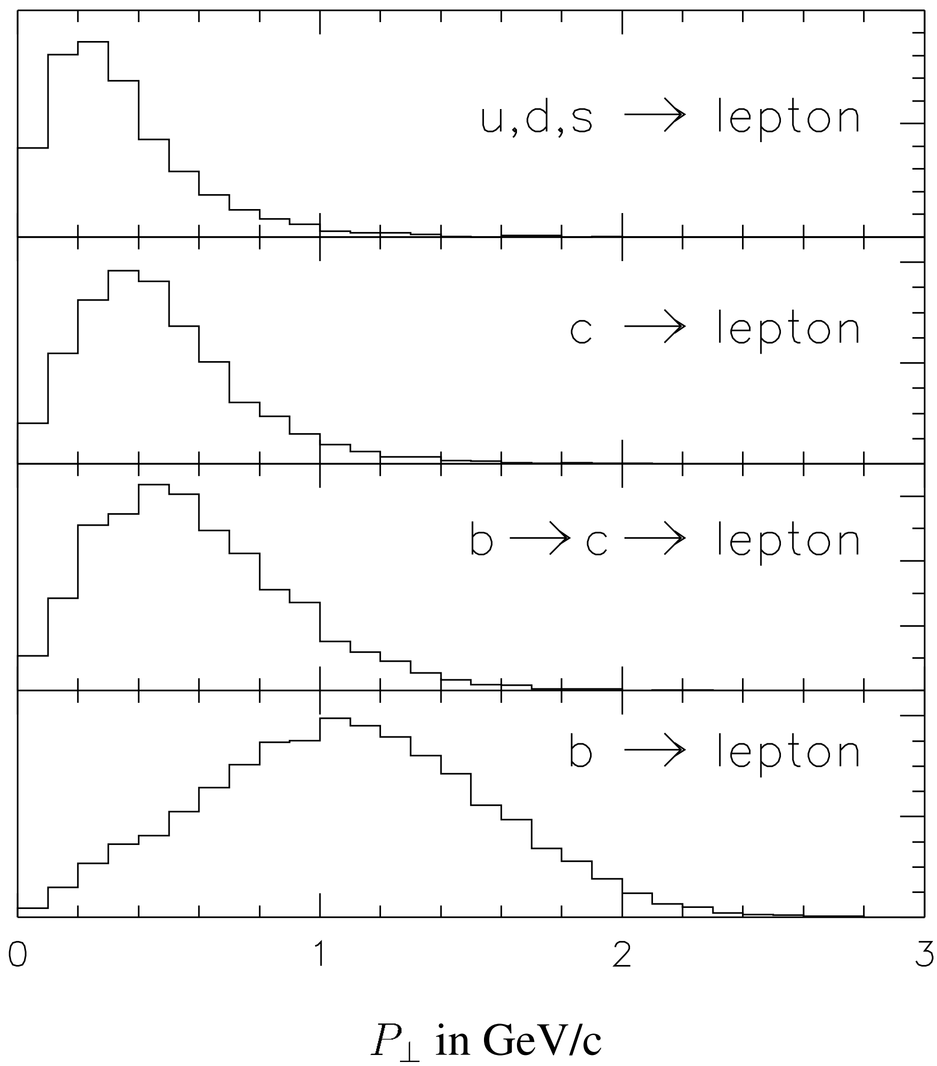

Figure 1.6: Transverse momentum spectra (in arbitrary unit) of leptons from different sources.

reconstruction of the c baryon.

The relative larger error on b baryon lifetime is mainly due to the poor statistics of the b baryon sample. The b baryon sample is selected using $\Lambda\ell^{\perp}$correlation in this dissertation and the lifetime is extracted from a maximum likelihood fit to the impact parameter distribution of the lepton tracks in the $\Lambda\ell^{\perp}$sample.

Chapter 2

The ALEPH Experiment at LEP

2.1 The LEP Storage Ring

The Large Electron Positron (LEP) accelerator at CERN has been described in detail elsewhere [28]. Only a brief description is given here. The LEP Collider is a 27 kilometer circumference circular electron-positron storage ring designed and constructed to accelerate, store, and collide electrons and positrons at up to 110 GeV (55 GeV per beam) center-of-mass (c.m.s.) energy at its first stage (LEP-I), and at up to about 180 GeV c.m.s. energy with a future upgrade. An overall view of LEP, with its injector chain, the storage ring, and the interaction sites, is shown in Figure 2.1.

Before entering the main LEP ring, the electrons and positrons are produced, accumulated, and accelerated to about 22 GeV in the injector complex consisting of LIL (LEP Injector Linac), EPA (Electron Positron Accumulator), and two synchrotrons PS and SPS. The beams are then further accelerated by the supercon-

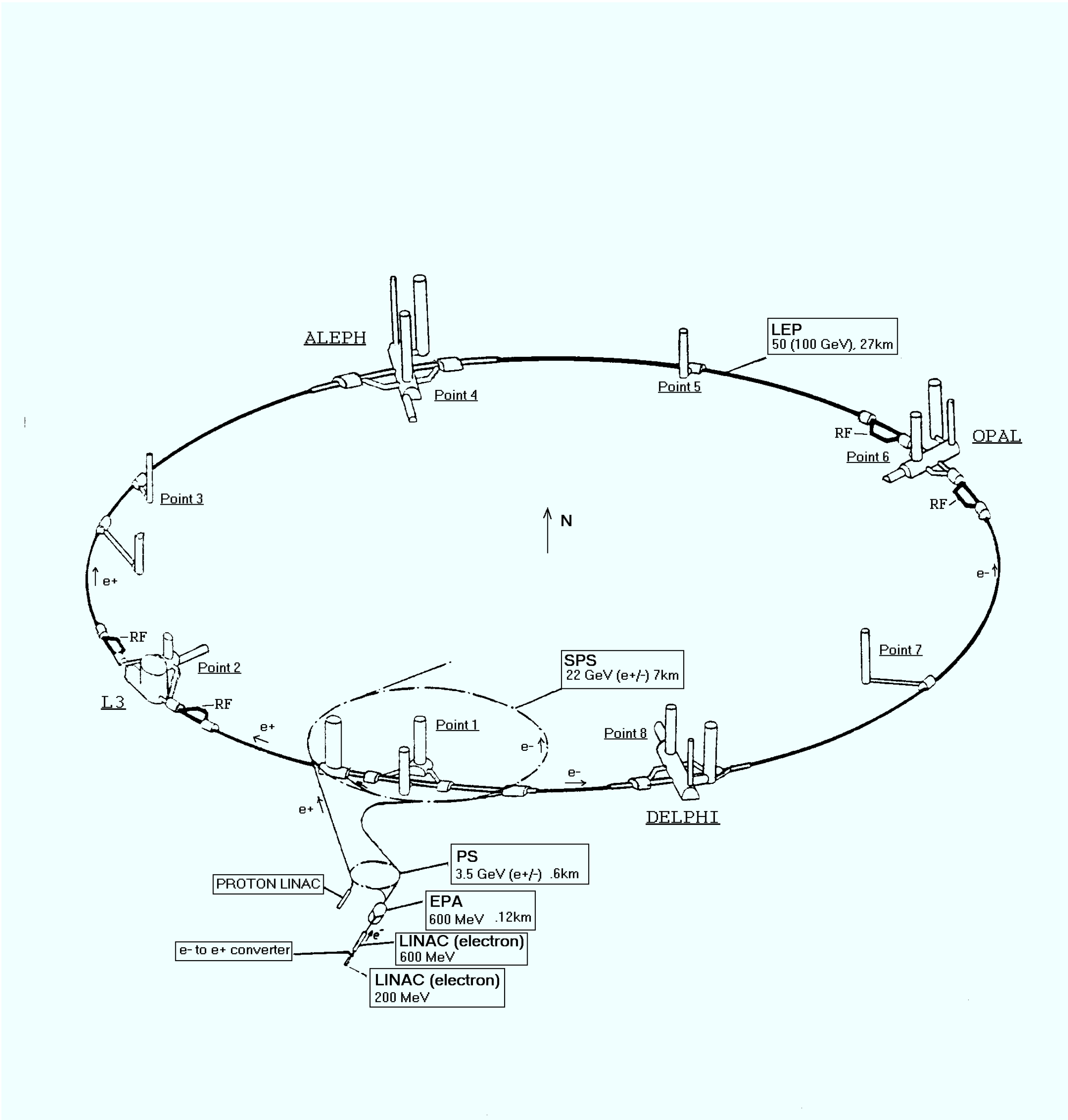

Figure 2.1: An overall view of LEP, its injector chain, the storage ring, and the interaction sites.

ducting RF cavities in the main LEP ring. After reaching the desired energy, the beams are squeezed and focused into collisions. Four bunches of counterrotating electron and positron beams are provided simultaneously by the machine for the collisions.

The LEP Collider at CERN has been producing $e^+e^\perp$ collisions in the energy vicinity of the Z boson mass peak since 1989 and is a copious source of heavy quarks from Z decays. Collisions at LEP can take place at up to eight interaction points spaced at equal intervals around the circular collider. Currently four of these interaction points contain large detectors to study the decays of the Z bosons produced by the $e^+e^\perp$ collisions; ALEPH (Apparatus for LEP PHysics) is one of these four detectors.

2.2 The ALEPH Detector

The ALEPH detector (Figure 2.2) is designed to perform a wide range of physics analyses. This goal requires high granularity, to ensure adequately detailed data about each event, and good hermeticity around the interaction region. These requirements are met with a variety of detector subsystems. The detector is composed of three major subsystems: the tracking detectors, the superconducting magnet which provides a homogeneous high magnetic field of 15000 Gauss for the tracking, and the calorimeters. They work together to produce a complete picture of each event.

The section below describes some of the main components related to this analysis. More detailed information, including the descriptions of the magnet, the

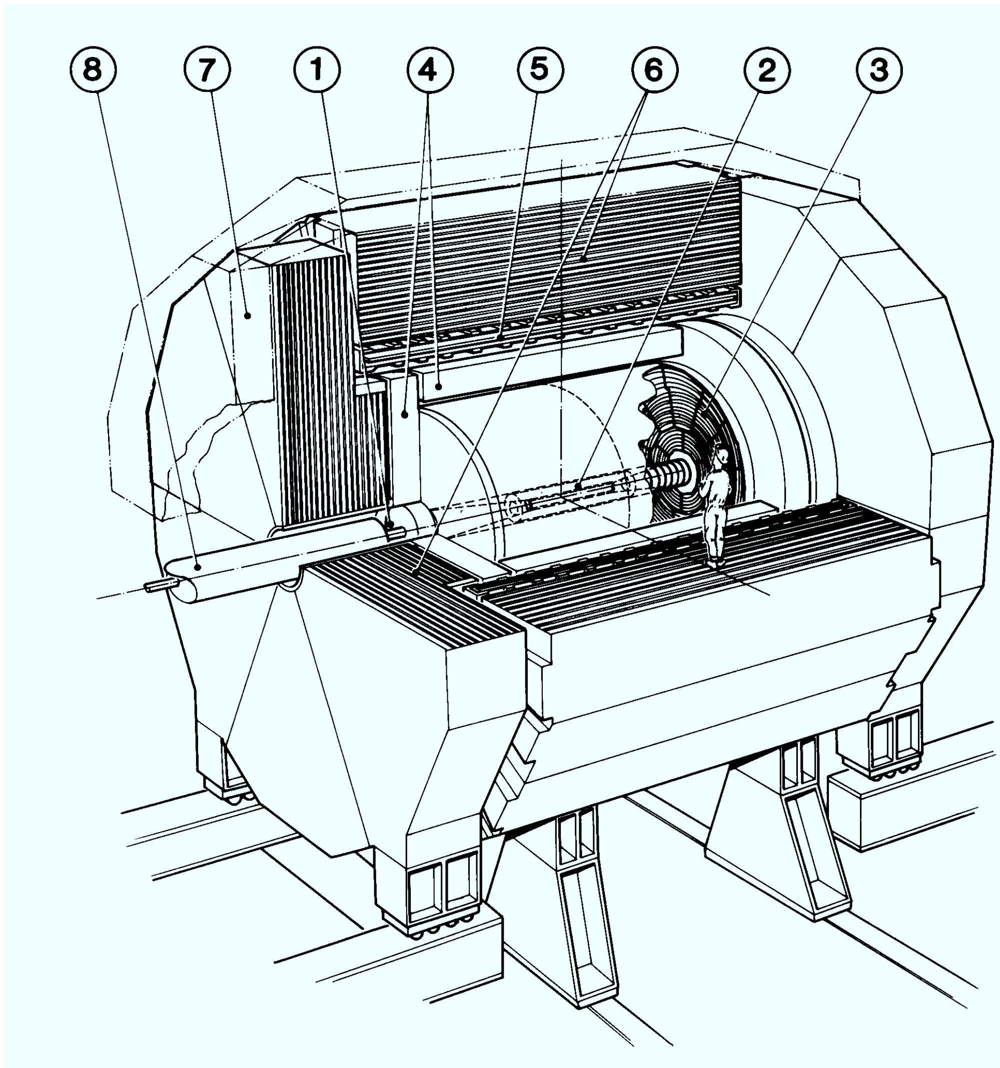

Figure 2.2: The ALEPH detector. 1) Luminosity monitor 2) Inner tracking chamber 3) Time projection chamber 4) Electromagnetic calorimeter 5) Superconducting coil 6) Hadronic calorimeter 7) Muon chamber 8) Low-beta superconducting quadrupoles.

electronics, the triggering system, the luminosity measurements and the performance of the detectors can be found in [29].

2.2.1 The Vertex Detector

The innermost of the ALEPH tracking detector is the silicon microvertex detector (VDET) (Figure 2.3). It consists of two concentric barrels of double-sided silicon microstrip detectors. The VDET was built and installed early in 1991. For this reason only data taken since 1991 was used in the analysis presented in this dissertation.

The basic structural unit of the VDET is the wafer, a 5 $\times$ 5 cm silicon crystal, 300 μm thick. Aluminized strips are implanted on both sides of the wafer with a pitch of 25 μm and a readout pitch of 100 μm. During operation, the strips on the two sides of the wafer are maintained at the voltage difference required to deplete the silicon of mobile charge carriers, varying by module between 16 and 80 V. A particle passing through the wafer liberates a set of electron-hole pairs, which drift to the two sides of the detector, giving a pulse on both sets of strips. A true three-dimensional point thus can be obtained.

The inner layer is composed of 9 elementary detector units (“faces") at an average distance of 6.3 cm, providing polar angle coverage to $\pm 58^0$ from the vertical. The outer layer is composed of 15 faces at an average radial distance of 10.8 cm, providing polar angle coverage to $\pm 44^0$ from the vertical. The spatial resolution is 12 μm in $r\phi$ and 12 μm in z for perpendicularly incident tracks. The impact parameter resolution and the momentum resolution have been studied

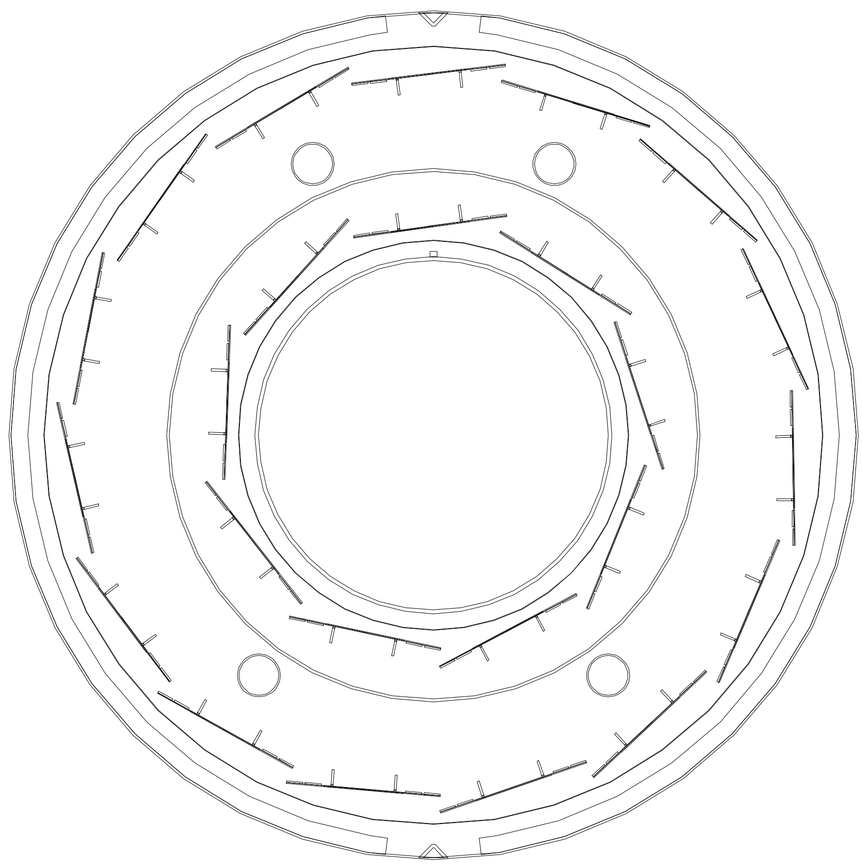

Figure 2.3: Schematic diagram indicating arrangement of the active area of the faces in the VDET geometry.

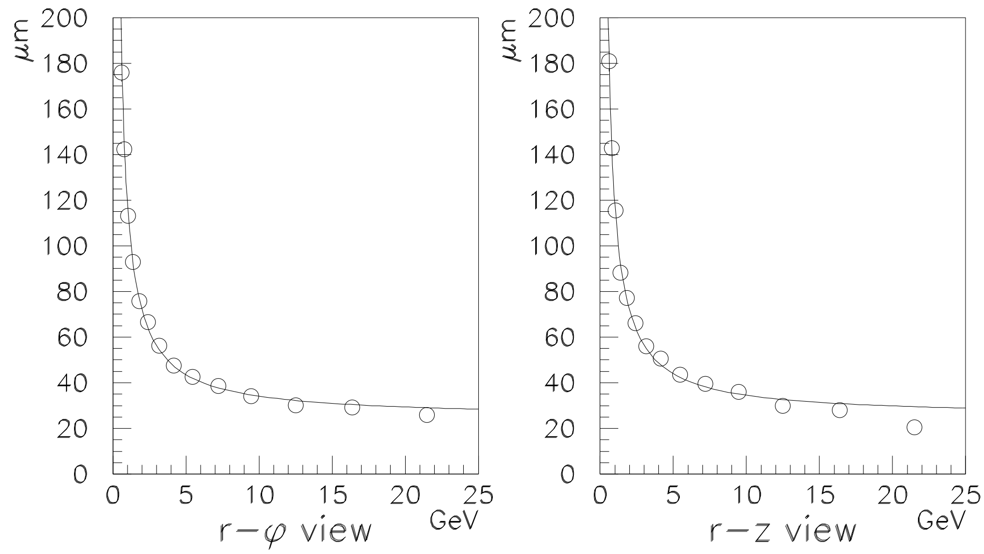

Figure 2.4: the resolution of impact parameter of tracks measured by the tracking detectors (include VDET) as a function of the track momentum.

with Z→ $\mu^+\mu^\perp$ events [30]. With tracks measured only by the Inner Tracking Chamber and the Time Projection Chamber, the impact parameter resolutions are 107 μm in $r\phi$ and 820 μm in rz, and the transverse momentum resolution is given by $\Delta P_\perp / P_\perp^2$ = 0.8 $\times 10^{\perp 3}$(GeV/c)$^{\perp 1}$. When the VDET is added, the impact parameter resolutions are 25 μm in $r\phi$ and 29 μm in rz, and the momentum resolution is $\Delta P_\perp / P_\perp^2$ = 0.6 $\times 10^{\perp 3}$(GeV/c)$^{\perp 1}$. Figure 2.4 shows the resolution of impact parameter of tracks as a function of the track momentum.

2.2.2 The Inner Tracking Chamber

The Inner Tracking Chamber (ITC) is a conventional wire drift chamber consisting of 8 concentric layers of sense wires located at radii between 12.8 and 28.8 cm and gives an average point resolution of 150 μm; the active length in z is 2 m, thus tracks with $|cos\theta|$ <0.97 will travel through all layers.

The z coordinate can be obtained by measuring the difference in the arrival times of pulses at the two ends of each sense wire, giving a precision of about 3 cm. There are a total of 960 sense wires which are operated at a positive potential in the range 2.0 $\perp$ 2.5 kV. Each sense wire is surrounded by six field wires which are held at ground potential. The maximum drift distance is 6.5 mm which means that all 960 sense wires can be read out in 500 ns, allowing the ITC to be used in the first-level trigger.

2.2.3 The Time Projection Chamber

Surrounding the ITC is the main tracking device, a large cylindrical time projection chamber (TPC). Measuring 4.4 meters in length and 3.6 meters in diameter, the TPC records up to 21 three-dimensional coordinates for each charged particle. This yields precise measurements of the momenta of the tracks, and also provides very good two track separation capability. With the magnetic field provided, a track momentum measurement accuracy of $\Delta P_{\perp}/P_{\perp}^{2}$ = 1.2 $\times 10^{\perp 3}$(GeV/c)$^{\perp 1}$. is made possible by the TPC alone. A schematic picture of the TPC is shown in Figure 2.5.

The TPC also records energy loss (dE/dx) information of the tracks through its

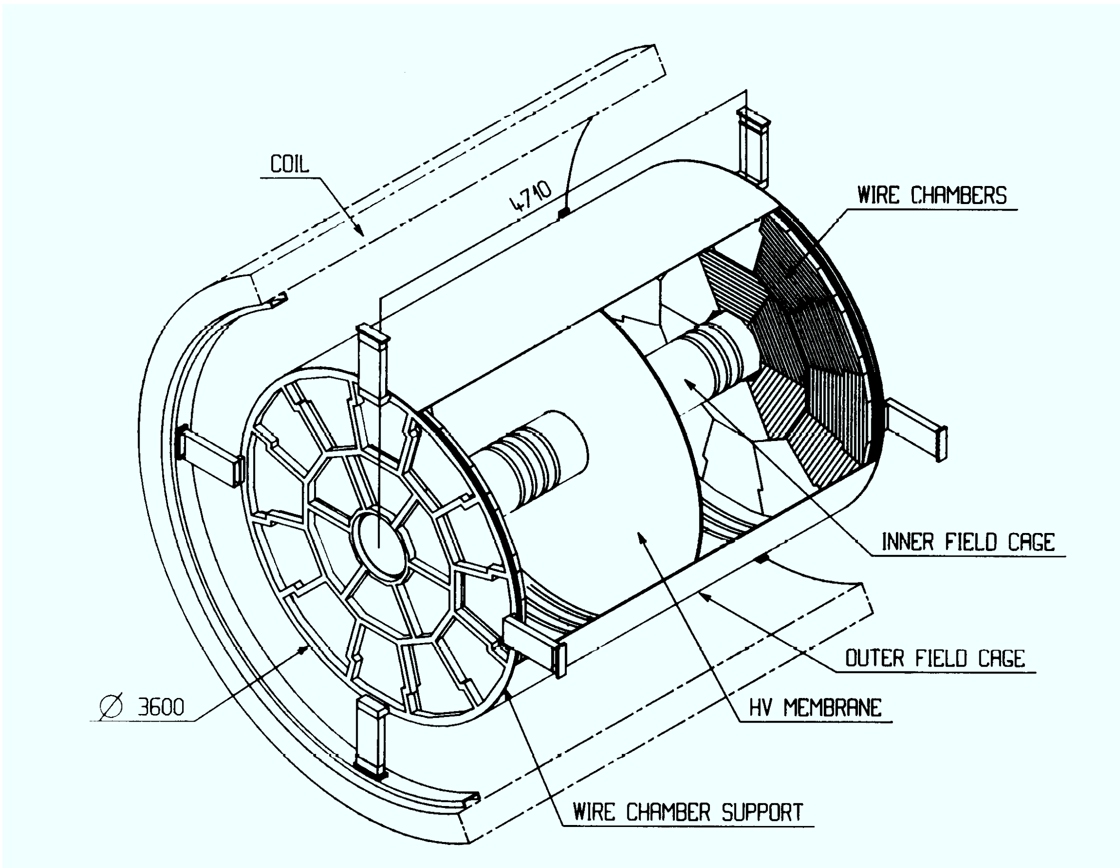

Figure 2.5: The Time Projection Chamber.

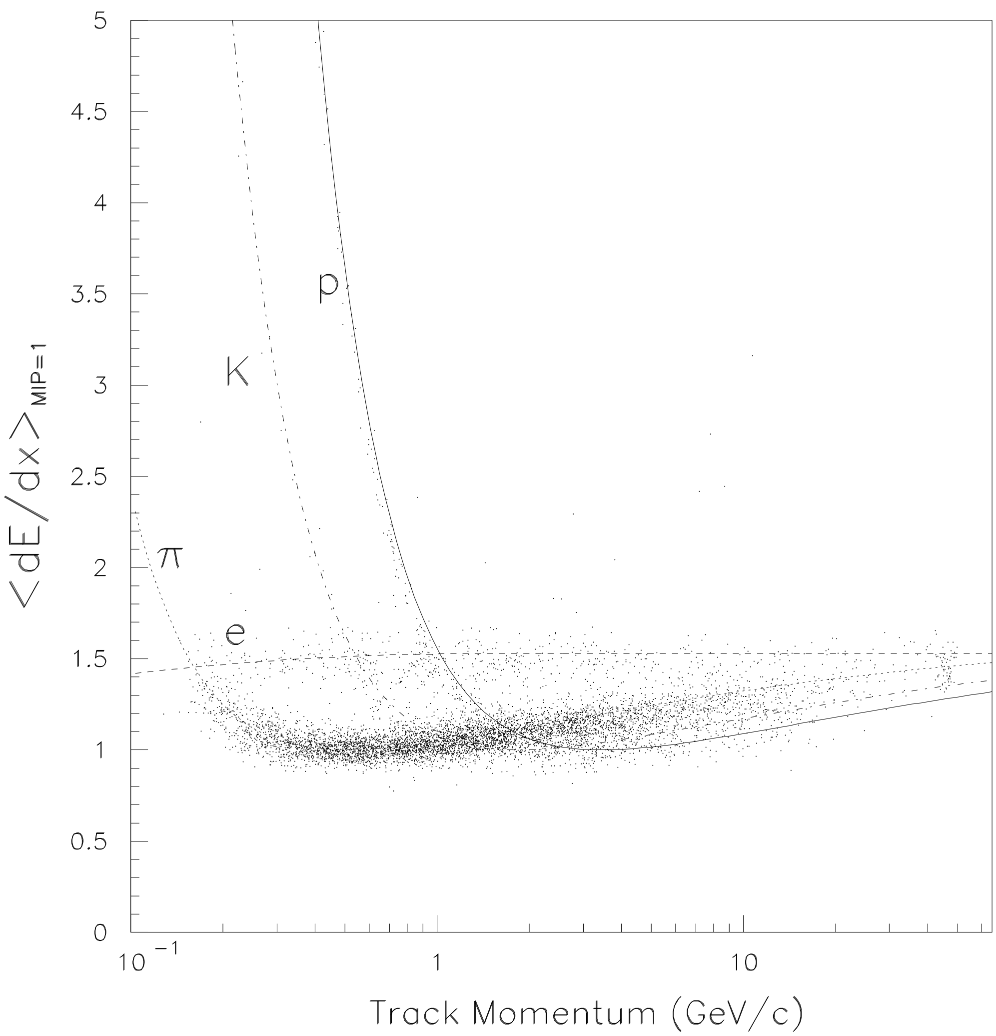

Figure 2.6: dE/dx versus momentum P for the tracks in a sample of Monte Carlo Z decays. Tracks are required to have at least 80 wire hits. The value of dE/dx is normalized to 1 for minimum ionization pions. Lines are the expected values for electrons (dash), pions (dot), kaons (dot-dash), and protons (solid).

measurements of up to 340 samples of the ionization for each track. This provides a powerful technique for particle identification, especially in separating electrons from pions. Figure 2.6 shows the dE/dx of tracks from Z decays plotted against the momentum P in GeV/c. The lines are those expected for electrons, pions, kaons, and protons. In the low energy region (< 10 GeV/c) the pions and the electrons are well separated. The TPC dE/dx resolution is about 4.5% for Bhabha electrons.

2.2.4 The Electromagnetic Calorimeter

Outside the TPC, but inside the magnet coil, is the electromagnetic calorimeter (ECAL). The thirty six ECAL modules, mounted both in the barrel and endcap regions surrounding the TPC and covering 3.9π of solid angle, are each made up of 45 alternating layers of lead and wire proportional chambers. In depth, this represents 22 radiation lengths (X_0), large enough to absorb all the electromagnetic energy carried by photons and electrons.

To measure the energy and the position of electromagnetic showers, small cathode readout pads are placed throughout each layer of wire chambers. In readout, the pads are internally connected to form so-called "towers" pointing towards the interaction point. Each tower is about $1^0 \times 1^0$ in angular size and produces three readouts for the first 10 layers (the first "stack", corresponding to $4X_0$), the next 23 layers (the second stack, $9X_0$), and the last 12 layers (the third stack, $9X_0$). This arrangement, yielding $18\%/\sqrt{E}$ (GeV) for the energy resolution, also provides a highly granular means to determine the shower positions and to do the pattern recognition. In addition, each wire chamber is read out separately in every module. These wire signals have very high sensitivities and are used as part of trigger signals.

2.2.5 The Hadron Calorimeter and the Muon Detector

Another calorimeter, the hadron calorimeter (HCAL) measures hadronic showers Like the ECAL, the HCAL has a layered sandwich structure, in which iron sheets and limited streamer tubes are placed in each of the twenty three layers. The whole structure has more than seven interaction lengths and is located just outside the magnet. It also serves as the return yoke of the magnetic coil. As an extension to the HCAL, a structure of two additional double layers of streamer tubes are separately mounted outside it to measure the muons penetrating the HCAL. These layers are called the muon detector.

Just like the ECAL, the HCAL is divided into modules. Each module has readouts from the wires and the localized pads, which are also connected in towers. In addition, aluminum strips are placed parallel to the wires on one side of each streamer tube. These strips couple capacitively to the wires to provide a third source of signals.

2.2.6 The ALEPH Trigger

The ALEPH trigger system has three levels. The Level 1 trigger is based on the ITC, ECAL and HCAL, and makes its decision within 5 μs (compared to 22 μs between two beam crossings). Level 1 reduces the trigger rate to a few Hz. If Level 1 triggered, the TPC is read out. The Level 2 trigger decision is identical to the Level 1 trigger, except that the ITC tracks are replaced by TPC tracks. If Level 2 is triggered, the entire detector is read out and a partial event reconstruction is performed. The Level 3 trigger is based on this partial event reconstruction, and uses correlations between the subdetectors to screen out false triggers and cosmic ray events. The ALEPH trigger system is virtually 100% efficient for hadronic Z decays.

2.3 Event Reconstruction in ALEPH

The raw data collected by the ALEPH detector is converted to a format suitable for offline analysis by the reconstruction program JULIA (Job to Unveil LEP Interactions in ALEPH). The main tasks of JULIA are as follows:

- Converting pulses recorded by the VDET, ITC and TPC into spatial track coordinates, and associating these coordinates to form tracks;
- Obtaining dE/dx information for the tracks by associating the tracks with wire data recorded by the TPC;
- Grouping together energy deposits in the calorimeters into clusters;
- Extrapolating of tracks through the calorimeters and associating of the calorimeter clusters with the tracks;
- Analyzing the shape and structure of ECAL clusters and calculating of variables to be used for electron and photon identification;

- Analyzing the hits in the HCAL and Muon Chambers for muon identification;

- Identificating pairs of oppositely charged tracks from the conversion of photons into $e^+e^\perp$ and other neutral particle decays like $\mathrm{K}^0_\mathrm{s} \rightarrow \pi^+\pi^\perp$, $\Lambda \rightarrow \mathrm{p}\pi^\perp$.

- Reconstructing small-angle Bhabha events in the Luminosity (LCAL) and the Small-Angle Tracker (SICAL);

- Calculating of the primary interaction point using the charged tracks;

Only a very brief introduction to the relevant topics of dissertation are described in this chapter.

2.3.1 Track Reconstruction and Performance of the Tracking System

The reconstruction of tracks in ALEPH is composed of pattern recognition and the global track fit. The pattern recognition begins at the outer layers of the TPC where the tracks are best separated. The algorithm finds sets of three hits in the rows of TPC pads which are consistent with lying along a helix, and extrapolates the helix inward towards the center of the detector by adding additional hits within the road and updating the estimated helix parameters along the way. The track extrapolation using the TPC and ITC has an uncertainty of approximately 200 μm in $r\phi$ which is much larger than the approximately 12 μm resolution of the

VDET hits. This will result in some ambiguities in the association of the tracks to VDET hits. There is also ambiguity due to the fact that the VDET module consists of two perpendicular strip detectors rather than a pixel device. However, the incident angles of the tracks are well measured by the TPC+ITC system to the order of 1 mrad, and this helps to remove the ambiguities in interpreting the VDET information.

The helix parameters are determined for each track using a Kalman filter algorithm [31]. It finds the best estimate of the track parameters and then updates them each time a new reading of the trajectory is available.

High momentum $\mu^+\mu^\perp$ pairs which have an energy equal to that of the beam are used to measure the momentum resolution and spatial resolution of the tracking system. For tracks measured only by the ITC and the TPC, the impact parameter resolutions are 107 μm in $r\phi$ and 820 μm in rz, and the momentum resolution is given by $\Delta P_\perp / P_\perp^2$ = 0.8 $\times 10^{\perp 3}$(GeV/c)$^{\perp 1}$. When the VDET is included, the impact parameter resolutions are 25 μm in $r\phi$ and 29 μm in rz, and the momentum resolution is $\Delta P_\perp / P_\perp^2$ = 0.6 $\times 10^{\perp 3}$(GeV/c)$^{\perp 1}$.

2.3.2 Interaction Point Reconstruction

The interaction point reconstruction algorithm operates on an event-by-event basis. The method [32] is designed to remove the effect of tracks which result from the decay of particles with measurable lifetimes, particularly $c\bar{c}$ and $b\bar{b}$ hadrons. Jets are created out of tracks and calorimeter clusters. For each jet, the tracks in the jet are projected into the plane perpendicular to the jet direction. To first order the effect of the lifetime of the hadron is removed in this plane. An estimate of the point of origin of the tracks in this two-dimensional projection is made by χ^2 minimization. In addition to the tracks in the event, a strong constraint on the location of the interaction point comes from the beam centroid and its error ellipse. In order to reduce the bias introduced when the jet direction does not approximate well the direction of the parent b or c hadron, only jets with a momentum of more than 10 GeV/c, and lying within $|\cos(\theta)| < 0.95$ are used. This algorithm has a resolution of 50μm $\times$ 10μm $\times$ 60μm for Z $\rightarrow$ $\mathrm{b\bar{b}}$ events, and a resolution of 40μm $\times$ 10μm $\times$ 50μm for events with Z decays into $\mathrm{u\bar{u}}$, $\mathrm{d\bar{d}}$ or $\mathrm{s\bar{s}}$.

2.3.3 Λ Reconstruction

Λ ($\bar{\Lambda}$) candidates are identified by their decay $\Lambda \rightarrow \mathrm{p}\pi^{\perp}$ ($\bar{\Lambda} \rightarrow \bar{\mathrm{p}}\pi^{+}$). As Λ has a very long lifetime ($c\tau$ = 7.89cm [5]), most Λ decays to p$\pi^{\perp}$ appear in the middle of the detector as topologically displaced vertices. Displaced vertices are found using an algorithm [33] which tries to make a vertex from each pair of oppositely-charged tracks, both of which have at least 4 hits in the TPC. This algorithm first calculates an approximate vertex position from the intersection of the two helices projected onto the $r\phi$ plane and then perform a vertex fit using this approximate position as a starting point of the fit. To be considered as a displaced vertex, the resulting vertex must satisfy the following criteria:

- the fitted vertex must lie inside the fiducial volume of the tracking system;
- the χ^2 of the fit when both tracks are constrained to pass through the primary interaction point must be greater than 30; (i.e. they are not consistent with

coming from the primary interaction point.)

- the distance between the helices at their point of closest approach must be less then 2.0 cm in $r\phi$;
- the difference between the tangents of the polar angles of the points on the tracks corresponding to the point of the closest approach in the $r\phi$ plane must be less than 0.06;
- the χ^2 of the vertex fit must be less than 13;
- the angle between the vector from the primary interaction point to the vertex and the vector sum of the momenta of the two oppositely-charged tracks coming from the vertex must be less than 23^o.

The decay lengths of the neutral particles represented by these displaced vertices are calculated with respect to the primary interaction point. To reduce combinatorial background arising from tracks near the primary interaction point, only those Λ candidates with a decay length greater than 5 cm are considered. To reject the background from similar displaced vertices of other neutral particles ($\mathrm{K^0_s} \to \pi^+\pi^\perp$ and $\gamma \to e^+e^\perp$), vertices which are consistent with $\mathrm{K^0_s} \to \pi^+\pi^\perp$ mass hypothesis within 10 MeV or $\gamma \to e^+e^\perp$ mass hypothesis within 15 MeV are rejected. In cases where TPC dE/dx information is available, the measured ionization of the track is required to be consistent (within three standard deviations for the pion and two standard deviations for the proton) with the corresponding particle hypothesis to reduce the combinatorial background due to vertices in which one or both tracks are clearly identified as something other than a proton or pion. Figure 2.7 shows the efficiency for finding $\Lambda \to p\pi^{\perp}$ as a function of the Λ momentum, and Figure 2.8 shows the Λ mass peak found by the algorithm in the data. The Λ reconstruction efficiency is low for very low momenta Λ's, this is due to the low track reconstruction efficiency for the very soft $\pi^{\perp}$'s from $\Lambda \to p\pi^{\perp}$ decays. When the Λ is energetic, the boost is large and the Λ tends to travel longer in the TPC before it decays into $p\pi^{\perp}$, therefore the p and $\pi^{\perp}$ from Λ decay will have fewer TPC hits, which will also result in a low Λ reconstruction efficiency (Figure 2.7).

2.3.4 Electron Identification

Electrons are identified [34] by combining the dE/dx and momentum information measured by the TPC with the shower energy, shape and depth measured by the ECAL. Electrons produce electromagnetic showers in the ECAL which have a distinctive transverse and longitudinal profile. dE/dx measurements are most effective in separating electrons from other particles at low momenta (Figure 2.6) while the ECAL information is most effective at high momenta. As the electrons of interest in this dissertation come from semileptonic b decay, electrons from photon conversions or from Dalitz decays of the π^0 are considered as background and are removed by finding pairs of oppositely charged electron candidates that are consistent with coming from photon conversions.

Electrons with momenta greater than 2 GeV/c deposit most of their energy in the ECAL towers. Several quantities (called "estimators") are extracted from the ECAL signals to help the electron identification. One of them is called R_T, a

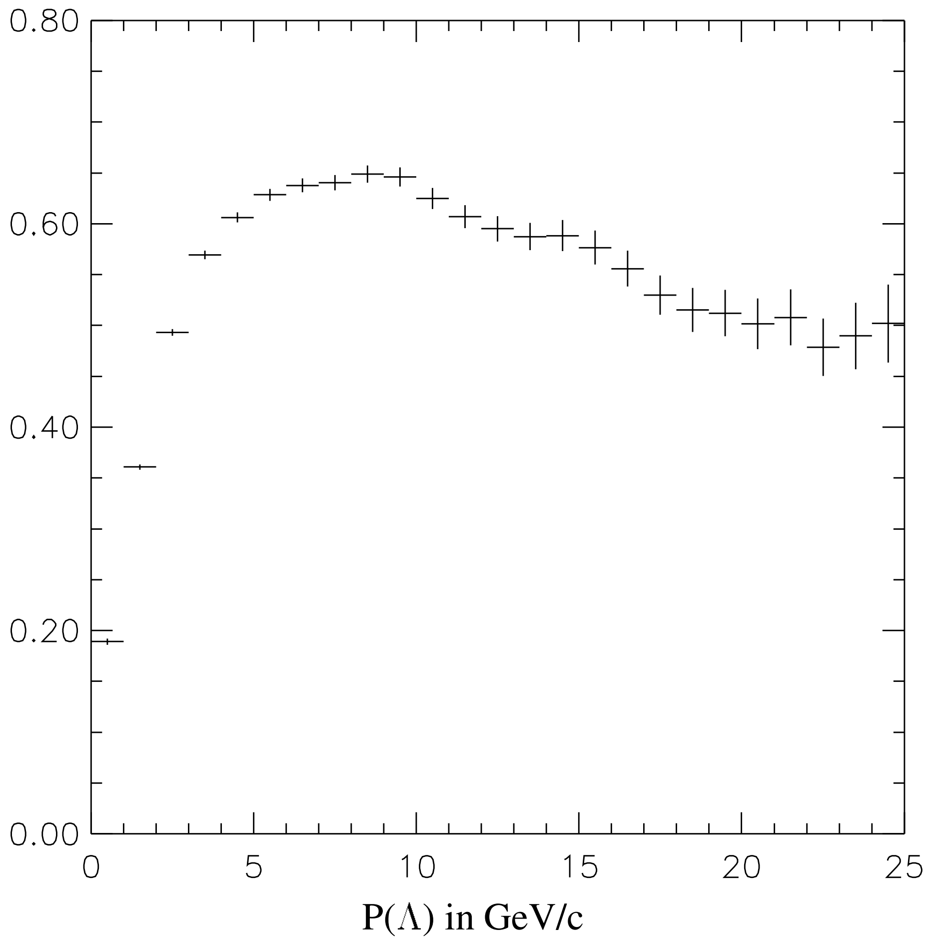

Figure 2.7: Λ reconstruction efficiency as a function of the Λ momentum.

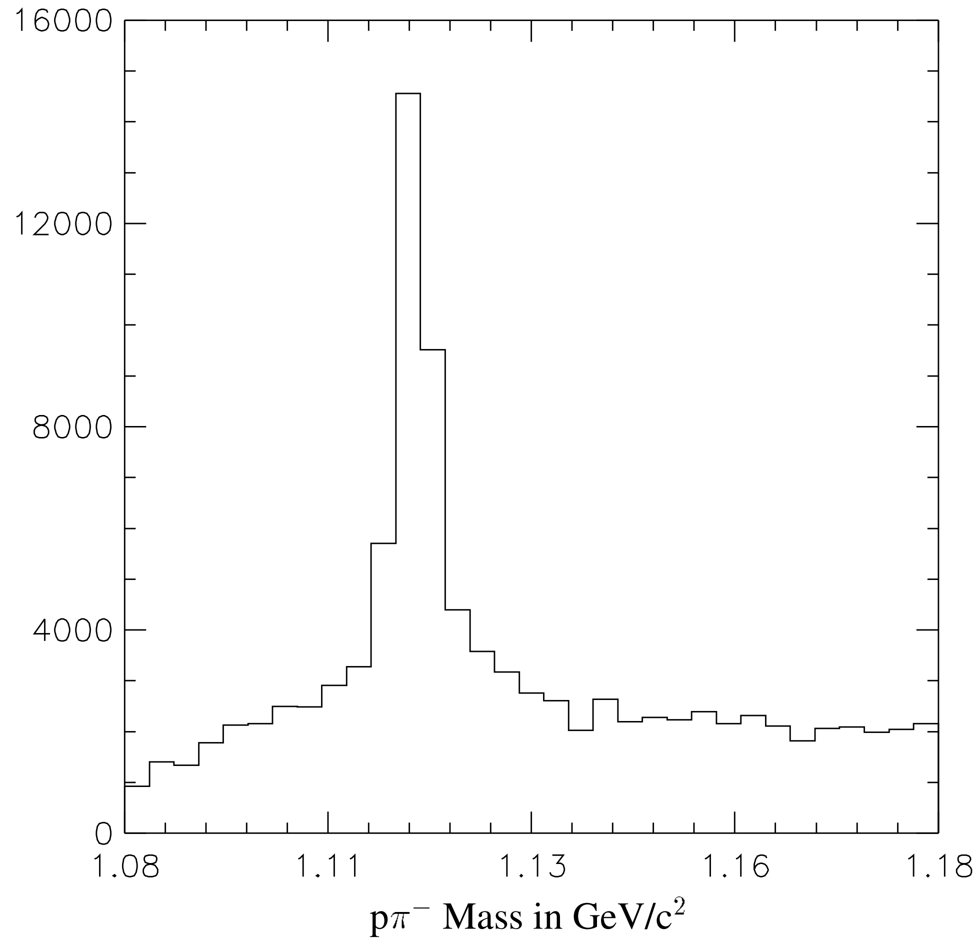

Figure 2.8: The $p\pi^{\perp}$ invariant mass distribution of the Λ candidates reconstructed in the data by the displaced vertices finding algorithm.

shower compactness estimator defined by:

$$R_T = \frac{X_{measured} \perp X_{expected}}{\sigma(X)},$$

where $X = E_0$/P and P is the momentum of the particle measured by the tracking devices. E_0 is the sum of the shower energy deposited in the three stacks of the four towers immediately surrounding the extrapolated trajectory of the track in the ECAL. If E_i is the shower energy deposited in the *i*th stack of these four towers, $E_0 = \sum_{i=1}^{3} E_i$. The $X_{expected}$ is determined from test beam to be 0.83, independent of the angle and the momentum, for electrons with P $>$ 2 GeV/c. The variance of X, $\sigma^2(X)$, is also obtained from the test-beam measurements and parametrized with respect to the momentum. For electrons, R_T is close to zero with a unit variance. For pions, R_T tends to be less than zero.

Another estimator called R_L is based on the longitudinal information of the shower associated to the track. Let S_i be the mean longitudinal position of the shower in stack *i*. A variable A is then defined as:

$$A = \frac{E_0}{\sum_{i=1}^{3} E_i S_i},$$

where E_0 and E_i are the same as defined before.

R_L is defined with respect to A just as R_T is to X:

$$R_L = \frac{A_{measured} \perp A_{expected}}{\sigma(A)}$$

Likewise, $A_{expected}$ and $\sigma^2(A)$ are obtained and parametrized from the test beam measurements.

The R_T and R_L prove to be very powerful in separating electrons and pions. Electron candidates are required to have $\perp$ 1.8 $< R_L <$ 3.0 and $R_T > \perp$ 1.6. Electrons can radiate photons in the inner tracking system, the ECAL may not have adequate spacial resolution to separate the photon's energy deposit from the electron's, resulting in large values of R_T. That is why there is no upper limit for R_T.

As mentioned before, the dE/dx method is very effective in separating the low momentum electrons and pions. The ionization measurements of the electron candidates are required to satisfy the loose requirement :

$$\frac{(\text{observed ionization} \perp \text{expected ionization})}{\text{resolution}} > \perp 2.5.$$

The overall electron identification efficiency is about 54%, based on a simulation of the ALEPH detector, with a hadron misidentification probability of about 0.07%. This yields a final electron purity of about 96%.

2.3.5 Muon Identification

Muons penetrate the detector material much more effectively than any other charged particles. Detailed information about muon identification can be found in reference [34]. Only a brief introduction is given here. The HCAL and muon chambers are used to separate narrow and penetrating ionization trails from the wide digital readout patterns of showering particles. Pions deposit their energy in broad showers that do not, in general, penetrate to the last layers of the HCAL, a distance of 7.5 interaction lengths. Muons penetrate the entire HCAL and leave hits in each layer.

Several quantities that distinguish between muons and hadrons are:

- Nexp, the number of planes expected to fire.
- Nfir, the number of planes which actually did fire.
- N_{10} the number of firing planes among the last ten expected planes.
- Xmult, the average hit multiplicity per firing plane for the last 11 planes.

The muon candidates are required to satisfy:

- Nexp > 10, to remove tracks passing through dead regions of the HCAL.
- Nfir/Nexp ≥ 0.4, to remove tracks which shower early.
- $N_{10} \geq 5$, to remove tracks which do not penetrate the outer part of the HCAL.
- Xmult ≤ 1.5, to remove tracks which shower late in the HCAL.

The muon candidates are also required to have at least 1 hit in the muon chamber. This cut is very powerful for background rejection. To ensure the muon penetrates the HCAL, only tracks with momentum greater than 3.0 GeV/c are considered for muon identification. The overall muon identification efficiency is about 76%, based on a simulation of the ALEPH detector, with a hadron misidentification probability of about 0.14%. This yields a final muon purity of about 87%.

Chapter 3

b Baryon Sample from Z Decays

Due to the low b baryon production and reconstruction rate, it is not practical to fully reconstruct the b baryons at LEP and measure the lifetime using the exclusive b baryon sample, with the present data sample. ALEPH published the first evidence for the semileptonic decay of b baryons, using $\Lambda\ell^{\perp}$ correlation identified in the data collected in the 1990 running period of LEP [21]. The result was confirmed later by other collaborations [22, 23]. In this chapter we first describe the method of $\Lambda\ell^{\perp}$ correlation and then the isolation of the b baryon sample.

3.1 $\Lambda\ell^{\perp}$ Correlation from b Baryon Decay

This method [21, 35] of using $\Lambda\ell^{\perp}$ correlation to identify a b baryon sample in Z decays takes advantage of the large semileptonic b decay rate ($Br(\mathrm{b} \to \mathrm{c}\ell^{\perp}\overline{\nu}) \simeq 21\%$) and the large branching ratio of $\Lambda_c^+ \to \Lambda X$ ($Br(\Lambda_c^+ \to \Lambda X) = (35 \pm 11)\%$) [5]. The Λ can decay to p$\pi^{\perp}$ with a branching ratio of $(64.1 \pm 0.5)\%$ [5]. In the decay of $\Lambda \rightarrow \mathrm{p}\pi^{\perp}$, the proton carries away most of the energy of the Λ. Therefore, $\Lambda \rightarrow \mathrm{p}\pi^{\perp}$ is easily distinguished from the decay $\overline{\Lambda} \rightarrow \overline{\mathrm{p}}\pi^{+}$; i.e. if the higher momentum track from the two-track vertex is positive, the vertex is a Λ candidate; if the higher momentum track is negative, the vertex is a $\overline{\Lambda}$ candidate.

b baryon decay gives $\Lambda\ell^{\perp}$ correlation as indicated in Figure 3.1, which shows the decay $\Lambda_{\mathrm{b}} \rightarrow \Lambda_{\mathrm{c}}^{+}\ell^{\perp}\overline{\nu}$, $\Lambda_{\mathrm{c}}^{+} \rightarrow \Lambda X$. As can be seen in the figure, Λ_{b} decays produce only $\Lambda\ell^{\perp}$ correlation. Charge conjugate decays are implied throughout this dissertation. In addition to Λ_{b}, other b baryons Ξ_{b} and Ω_{b} can also yield $\Lambda\ell^{\perp}$ correlation. However, as Ξ_{b} and Ω_{b} contain one or more s quarks, their production rate in Z decays is expected to be suppressed with respect to Λ_{b}. As mentioned in Chapter 1, Λ_{b} is used as a generic name for b baryons throughout this dissertation.

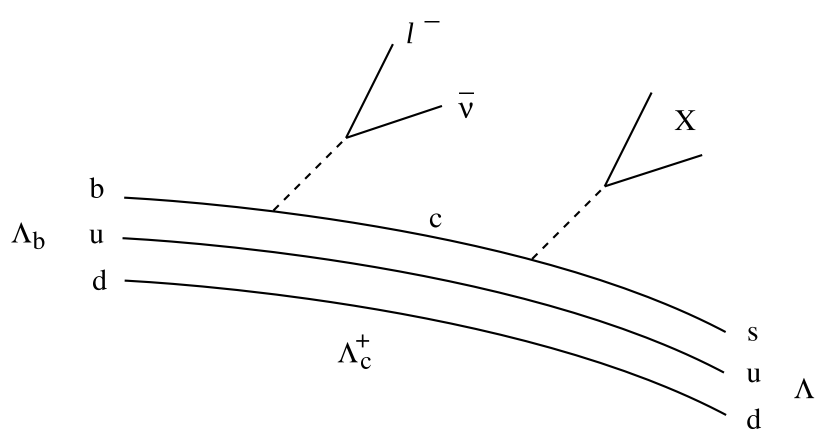

Figure 3.1: Quark constituents in the decay $\Lambda_{\mathrm{b}} \rightarrow \Lambda_{\mathrm{c}}^{+}\ell^{\perp}\overline{\nu}$ followed by $\Lambda_{\mathrm{c}}^{+} \rightarrow \Lambda X$.

3.2 Sources of $\Lambda\ell$ Combinations in Z Decays

Not all $\Lambda\ell^{\perp}$ combinations are from b baryon decays. There are six possible sources of $\Lambda\ell$ combinations:

$$\Lambda_{\mathrm{b}} \to \Lambda_{\mathrm{c}}^{+}\ell^{\perp}\overline{\nu},\ \ \Lambda_{\mathrm{c}}^{+} \to \Lambda X \tag{3.1}$$

$$\overline{\mathrm{B}} \to \Lambda_{\mathrm{c}}^{+}X\ell^{\perp}\overline{\nu},\ \ \Lambda_{\mathrm{c}}^{+} \to \Lambda X \tag{3.2}$$

$$\mathrm{b} \to \Lambda_{\mathrm{c}}^{+}D_{\mathrm{s}}^{\perp}X,\ \ \Lambda_{\mathrm{c}}^{+} \to \Lambda X, D_{\mathrm{s}}^{\perp} \to X\ell^{\perp}\overline{\nu} \tag{3.3}$$

$$\mathrm{b} \to \Lambda_{\mathrm{c}}^{+}X,\ \ \Lambda_{\mathrm{c}}^{+} \to \Lambda\ell^{+}X \tag{3.4}$$

$$\mathrm{c} \to \Lambda_{\mathrm{c}}^{+}X,\ \ \Lambda_{\mathrm{c}}^{+} \to \Lambda\ell^{+}X \tag{3.5}$$

$$\text{Accidental Combinations} \tag{3.6}$$

Processes (3.1) to (3.3) give $\Lambda\ell^{\perp}$ correlation, while processes (3.4) and (3.5) give $\Lambda\ell^{+}$ correlation. Process (3.6), representing the accidental combinations of real Λ's from fragmentation in association with real or fake leptons, contributes to both the $\Lambda\ell^{\perp}$ and $\Lambda\ell^{+}$ samples.

Leptons from processes (3.2) to (3.5) are expected to have low momentum and low transverse momentum comparing with leptons from our signal process (3.1), either due to the more than 3 body decay (processes (3.2) and (3.3)), or due to the fact that the lepton comes from c decay (process (3.3), (3.4) and (3.5)).

Figure 3.2 shows the lepton transverse momentum spectra of different processes that give $\Lambda\ell$ combinations from simulation. By requiring the lepton candidate to have at least 1 GeV/c of $P_{\perp}$ and 3 GeV/c of momentum, about 90% of the $\Lambda\ell$ correlation from process (3.2) and more than 95% of those from processes (3.3)

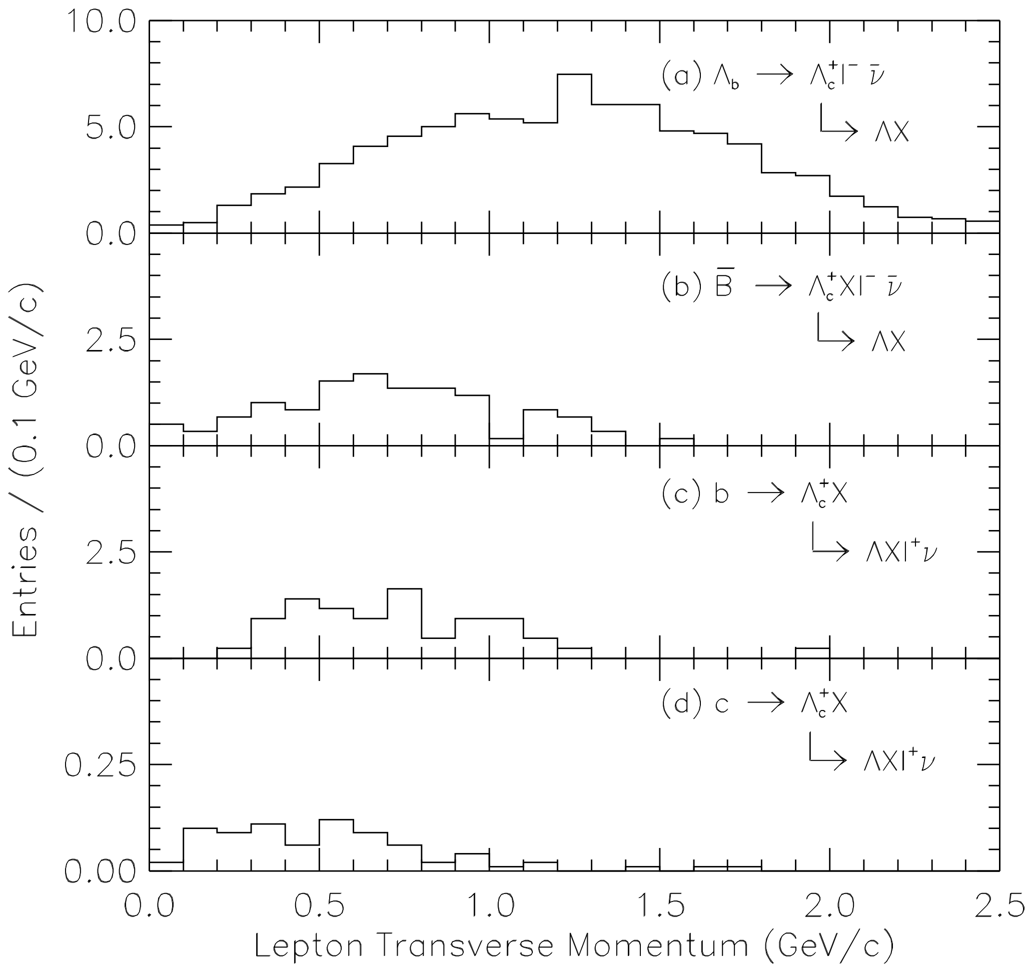

Figure 3.2: $P_\perp$ spectra of leptons from physics processes that give $\Lambda\ell$ combinations.

to (3.5) are removed, while keeping over half of the $\Lambda\ell^{\perp}$ correlation from b baryon decay. However, the accidental combinations cannot be completely removed with these lepton momentum and transverse momentum requirements, as the leptons in this process can really come from b decays (see Figure 1.6). To make sure the impact parameter of the lepton is well measured, the lepton candidates are further required to have at least one associated $r\phi$ coordinate in the VDET, five hits in the TPC and two hits in the ITC and a χ^2/d.o.f. for the track fit of less than 4. Lepton and Λ candidates are required to be within 45 degrees of each other.

To get rid of fake Λ's, fragmentation Λ's and other neutral particles like photon conversions and $\mathrm{K^0_s}$'s, the Λ candidate is required to have a momentum of at least 3.0 GeV/c, and to be identified by the Λ finding algorithm (Chapter 2). Figure 3.3 shows the momentum spectra of Λ's from b baryon decay and from fragmentation.

The remaining $\Lambda\ell^{\perp}$ combinations originate mostly from either b baryon semileptonic decays (3.1) or accidental combinations (3.6), while the $\Lambda\ell^{+}$ combinations are mostly accidental combinations (3.6) where the leptons are mainly from b decays plus real Λ from fragmentation.

Since the accidental $\Lambda\ell^{\perp}$ combinations cannot be removed, an estimate must be made of how many remain after all the selection criteria have been applied. As the production rate and momentum spectrum of the fragmentation Λ's in the Monte Carlo may not be very accurate, we can use the $\Lambda\ell^{+}$ combinations in the data to estimate the accidental $\Lambda\ell^{\perp}$ combinations, assuming that there is no significant correlation between the charge of the lepton and the fragmentation Λ. The validity of this assumption will be discussed later. The excess of $\Lambda\ell^{\perp}$ combinations over $\Lambda\ell^{+}$ is then taken to be due to semileptonic decay of b baryons.

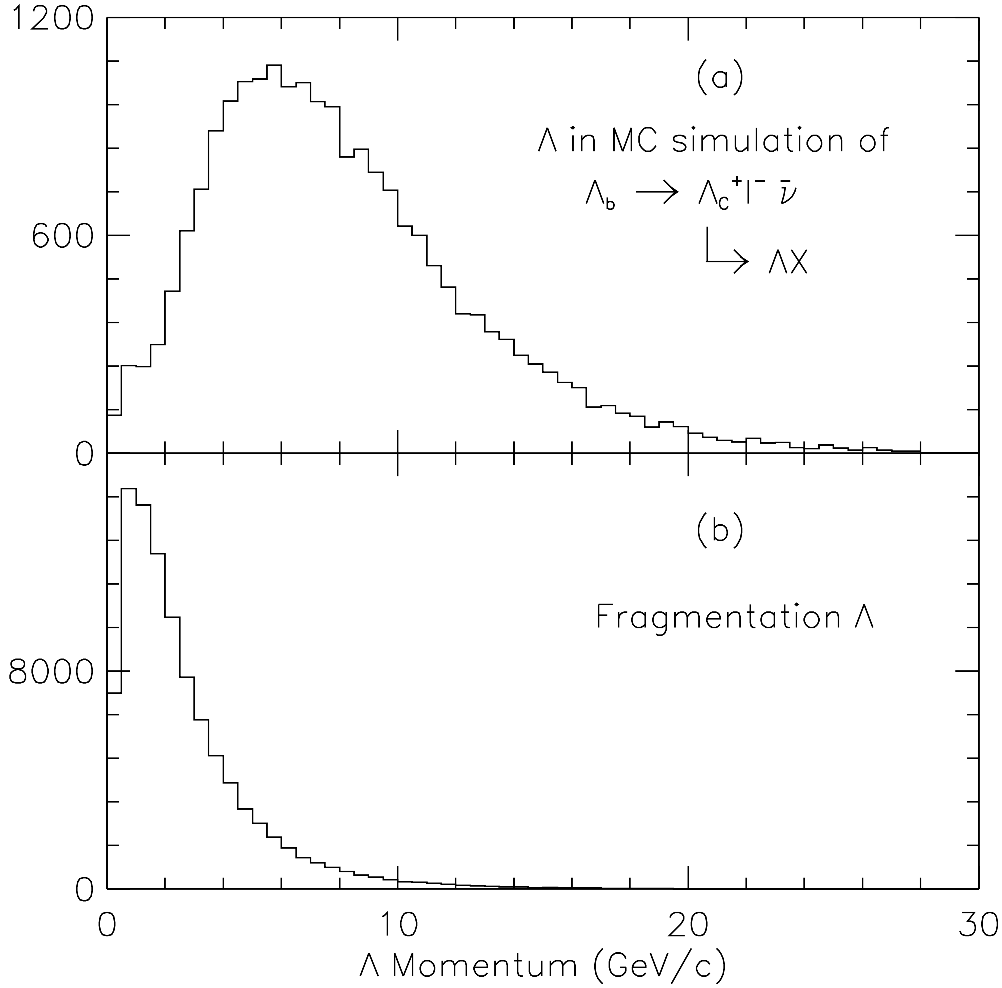

Figure 3.3: Momentum spectra of Λ's from b baryon decay and from fragmentation.

3.3 Analysis of the Data Sample

This analysis is based on data taken from 1991 to 1993, consisting of about 1,500,000 hadronic Z decays. The yields of $\Lambda\ell^{\perp}$ and $\Lambda\ell^{+}$ combinations, after application of the Λ and lepton selection criteria described above, are shown in Figure 3.4, where the $\mathrm{p}\pi^{\perp}$ invariant mass is plotted.

The two mass distributions are fitted using a Gaussian to represent the signal and a second order polynomial to represent the shape of the combinatoric background. The fit is performed to both distributions simultaneously, holding the means and widths of the two Gaussians equal. The resulting mass and width of the Gaussians are found to be 1115.6 ± 0.1 and 2.5 ± 0.1 MeV/c^2 respectively, consistent with the known Λ mass and expectations based on Monte Carlo simulation of the decay. The areas of the fitted Gaussians yield 441 ± 29 $\Lambda\ell^{\perp}$ combinations and 217 ± 24 $\Lambda\ell^{+}$ combinations. From this difference, a raw excess of 224 ± 38 $\Lambda\ell^{\perp}$ combinations is obtained. The $\Lambda\ell^{\perp}$ combinations with a $\mathrm{p}\pi^{\perp}$ invariant mass within two standard deviations of the nominal Λ mass are selected for the measurement of the b baryon lifetime.

3.4 Results and Discussion

To estimate the b baryon fraction in the $\Lambda\ell^{\perp}$ sample, the residual contributions of the background processes are evaluated. Based on a simulation of process (3.2), the 90% confidence level upper limit of $Br(\overline{\mathrm{B}} \to \mathrm{p}e^{\perp}\mathrm{X}) \leq 0.16\%$ set by the ARGUS collaboration [36] and the measured rate $Br(\Lambda_c^+ \to \mathrm{pX}) = (50 \pm 16)\%$

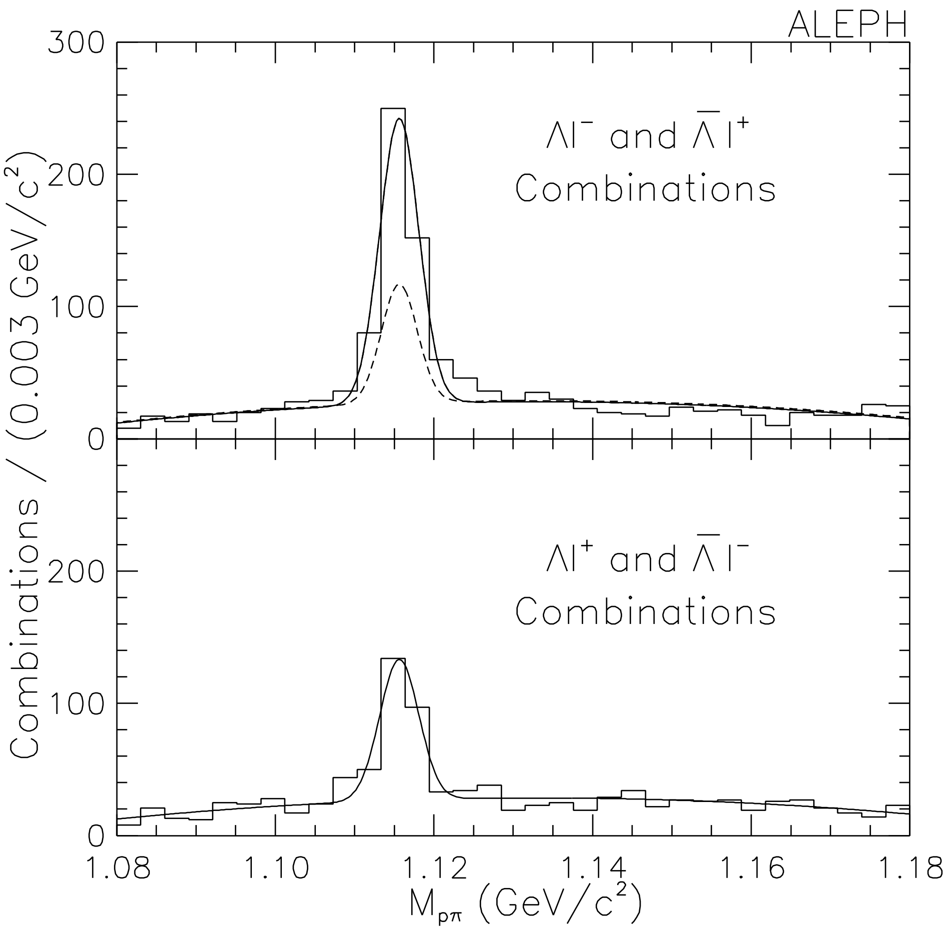

Figure 3.4: The p$\pi^{\perp}$ invariant mass distribution of the $\Lambda\ell^{\perp}$ and $\Lambda\ell^{+}$ combinations. The dashed curve represents the background level in the $\Lambda\ell^{\perp}$ (right sign) combinations estimated by the $\Lambda\ell^{+}$ (wrong sign) combinations after correction.

[5], less than 13 $\Lambda\ell^{\perp}$ combinations from this process are expected. This possible contribution is included in the systematic error on the measurement of the b baryon production rate and lifetime.

From a study of approximately 1.6×10^6 Z$\rightarrow$ $\mathrm{q\overline{q}}$ events generated with the JETSET 7.3 Monte Carlo, the contribution to the $\Lambda\ell^{+}$ sample from processes (3.4) and (3.5) is estimated to be 28 ± 5 combinations, which is subtracted from the wrong sign peak as a correction to the accidental combinations in the wrong sign peak. The contribution from process (3.3) is negligible.

Concerning the assumption that there is no significant correlation between the charge of the lepton and the fragmentation Λ, this is true if the accidental combination is the pairing of a fragmentation Λ with a fake lepton, i.e. such accidental combinations produce $\Lambda\ell^{\perp}$ and $\Lambda\ell^{+}$ combinations in equal numbers. However, if the accidental combinations is due to the pairing of a Λ from fragmentation with a genuine lepton from b quark decay, the value of the ratio in question, i.e.

$$\frac{\#\Lambda\ell^{-}}{\#\Lambda\ell^{+}}\Big|_{fragmentation\Lambda,\mathrm{b}\rightarrow\ell}$$

will depend on Br(b $\rightarrow$ baryons) in the Lund model. Figure 3.5(a) shows the fragmentation associated with the formation of a b meson in the Lund Model. To form a meson, the b quark must join with an antiquark from a quark-antiquark pair in the sea. The leftover quark from the pair, if it is to hadronize as a baryon, must join with the diquark of a diquark-antidiquark pair, leaving the antidiquark free to hadronize as an antibaryon to conserve the baryon number. If the baryon and antibaryon are Λ's, when they are combined with the negative lepton from the semileptonic decay of the initial b quark, will produce one $\Lambda\ell^{\perp}$ and one $\overline{\Lambda}\ell^{\perp}$ (i.e.

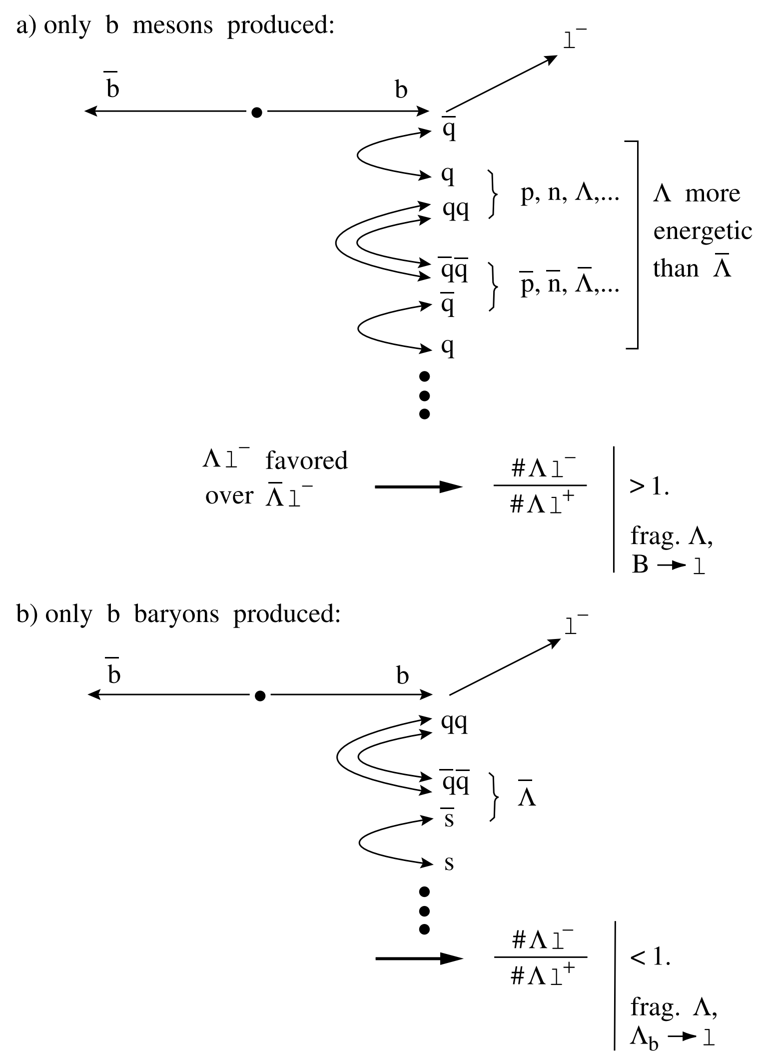

Figure 3.5: The formation of accidental $\Lambda\ell$ combinations during the fragmentation in associated with the formation of b hadrons in the Lund model: (a) the b quark hadronizes as a meson; accidental $\Lambda\ell^{\perp}$ and $\Lambda\ell^{+}$ combinations are formed, then the $\Lambda\ell^{\perp}$ combinations are more easily detectable; (b) the b quark hadronizes as a baryon; accidental $\Lambda\ell^{+}$ combinations are formed.

$\Lambda\ell^{+}$). However, the Λ in the $\Lambda\ell^{\perp}$ combination has higher momentum than the $\overline{\Lambda}$ in the $\overline{\Lambda}\ell^{\perp}$ (i.e. $\Lambda\ell^{+}$) combination and is therefore more likely to be detected. Therefore,

$$\frac{\#\Lambda\ell^{-}}{\#\Lambda\ell^{+}}\,|_{fragmentation\Lambda,\mathrm{b}\to\ell} > 1.0$$

Figure 3.5(b) shows the fragmentation associated with the formation of a b baryon in the Lund Model. To form a baryon, the b quark must join with the diquark from a diquark-antidiquark pair from the sea. The leftover antidiquark from the pair then hadronizes as an antibaryon, perhaps a $\overline{\Lambda}$ to conserve the baryon number. In this case, if the $\overline{\Lambda}$ is detected along with the negative lepton from the semileptonic decay of the initial b baryon, a $\Lambda\ell^{+}$ combination is formed. This will result in:

$$\frac{\#\Lambda\ell^{-}}{\#\Lambda\ell^{+}}\,|_{fragmentation\Lambda,\mathrm{b}\to\ell} < 1.0$$

From a study of approximately 1.6×10^{6} Z$\to$ $\mathrm{q}\overline{\mathrm{q}}$ events generated with the JETSET 7.3 Monte Carlo, the ratio of $\Lambda\ell^{\perp}$ to $\Lambda\ell^{+}$ accidental combinations is taken to be 0.8 ± 0.2. The error reflects an uncertainty in the knowledge of the momentum spectra of the Λ baryons produced in the process of b or $\bar{\mathrm{b}}$ quark fragmentation and covers 5% $\leq$ BR(b $\to$ b baryon) $\leq$ 15% [37].

All the above considerations together imply a b baryon signal of 290 ± 35 (stat) $\pm\ 39$ (syst) events.

In order to calculate the product branching ratio, the efficiency of selecting these $\Lambda\ell^{\perp}$ combinations from b baryon decays needs to be estimated. The JETSET 7.3 prescription is used to model semileptonic b baryon decay as well as the decay $\Lambda_{\mathrm{c}}^{+} \to \Lambda X$. It is assumed that three-body decays such as $\Lambda_{\mathrm{b}} \to \Lambda_{\mathrm{c}}^{+}\ell^{\perp}\overline{\nu}$ dominate the semileptonic decay of b baryons. The b quarks produced in the decay of the Z are polarized, and some or all of this polarization could be retained in the subsequent hadronization of the b quark into a b baryon. A polarized b baryon has harder lepton momentum and $p_{\perp}$ spectrum, and consequently the overall signal detection efficiency is larger. A polarization of $(30^{+34}_{-30})\%$ [38] gives a detection efficiency of $(7.5 \pm 0.6)\%$, where the error includes uncertainty due to polarization.

Assuming the Standard Model value for the partial width of Z$\rightarrow$ $\mathrm{b\overline{b}}$ applying the above corrections yields a product branching ratio:

$$\mathrm{Br}(\mathrm{b} \rightarrow \Lambda_{\mathrm{b}}) \cdot \mathrm{Br}(\Lambda_{\mathrm{b}} \rightarrow \Lambda_{\mathrm{c}}^{+} \ell^{-} \overline{\nu} X) \cdot \mathrm{Br}(\Lambda_{\mathrm{c}}^{+} \rightarrow \Lambda X)$$

$$= (0.61 \pm 0.07(\mathrm{stat}) \pm 0.10(\mathrm{syst}))\%$$

This is consistent with and supersedes ALEPH's previously published values [10, 21].

Chapter 4

b Baryon Lifetime Measurement

The lifetime of b baryon is extracted from a maximum likelihood fit to the impact parameter distribution of the lepton candidates belonging to the $\Lambda l^{\perp}$ sample. The fitting procedure is similar to that used in the previous measurement of b baryon lifetime [10]. The expected impact parameter distribution used to perform the maximum likelihood fit to the lepton candidates is obtained by convoluting a resolution function, which characterizes the detector effects, with the so-called “physics functions" which describe the expected underlying impact parameter distributions of various lepton sources.

In this chapter, we discuss the lifetime estimator (i.e. the impact parameter of the lepton), the fractions and the expected impact parameter distributions of leptons from different sources (i.e. the “physics functions"), the impact parameter resolution function, the fit for b baryon lifetime, systematic checks and finally systematic errors of the b baryon lifetime measurement.

4.1 Lepton Impact Parameter

A sample containing b baryon is obtained as described in the previous chapter. The Λ and lepton identification requirements described in the previous subsection, together with a cut of 6 MeV/c^2 window around the Λ mass to select the p$\pi^{\perp}$ combinations, yield a final sample (including the combinatorial (fake) background under the Λ mass peak) of 519 $\Lambda\ell^{\perp}$ candidates. The b baryon fraction in this sample is about 58%.

To extract the lifetime of b baryon from this sample, a lifetime estimator must be chosen. A typical Λ_b decay resulting in a $\Lambda\ell^{\perp}$ combination is shown in Figure 4.1. The only tracks reconstructed from the decay are the lepton and the p$\pi^{\perp}$ coming from the Λ decay. The Λ travels on average approximately 50 cm before decaying into p$\pi^{\perp}$ in the detector, while the decay length of Λ_b is about 2.5 mm for a Λ_b lifetime of 1.3 ps. Furthermore, the Λ comes from Λ_c^+ decay vertex instead of Λ_b decay vertex. Due to the above reasons, the p$\pi^{\perp}$ from Λ decay can provide little information about the Λ_b decay vertex. Since the lepton comes directly from the Λ_b decay vertex, a logical choice for the lifetime estimator is then the impact parameter of the lepton in the $\Lambda\ell^{\perp}$ combinations.

The “lifetime-signed" impact parameter δ is defined as shown in Figure 4.2, where the reconstructed jet axis is taken to represent the Λ_b flight direction, and the interaction point is used to approximate the production point. The jet axis is calculated using the JADE scale-invariant-mass clustering algorithm [39], and is assumed to originate from the interaction point. The crossing point of the lepton track and the jet axis is then compared with the lepton's point of closest approach to

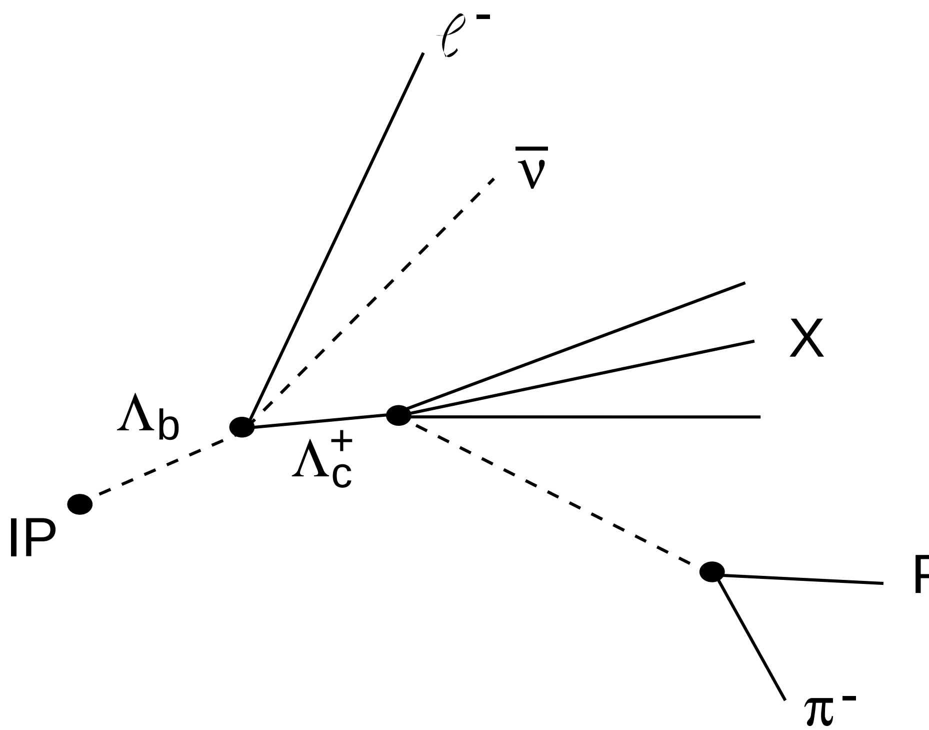

Figure 4.1: Topology diagram of the decay $\Lambda_{\rm b} \rightarrow \Lambda_{\rm c}^{+}\ell^{\perp}\overline{\nu}$ followed by $\Lambda_{\rm c}^{+} \rightarrow \Lambda X$ with $\Lambda \rightarrow {\rm p}\pi^{\perp}$

the interaction point. Defining “upstream" to be along the direction of the lepton’s momentum, if the track-jet crossing point is upstream from the point of closest approach to the origin, the impact parameter is signed positive. This corresponds to a track geometry consistent with the lepton coming from a long-lived particle, as for the solid track in Figure 4.2. The converse situation is assigned a negative impact parameter, as for the dashed track. If the true Λ_b direction and the actual production point were known, the impact parameter of the lepton from the Λ_b decay would always be positive.

4.2 Impact Parameter Distributions from Different Lepton Sources (Physics Functions)

The lepton impact parameter distribution in $\Lambda l^{\perp}$ combinations is described in the fit as a sum of different contributions from the possible sources of lepton:

- semileptonic decay of b baryon ($\Lambda_\mathrm{b} \to l$)
- semileptonic decay of generic b hadron (b $\to l$)
- cascade decays (b $\to$ c $(\tau) \to l$)
- c hadron decay in $\mathrm{c\bar{c}}$ events (c $\to l$)
- hadron misidentification (misid)
- π, K decay in flight or γ conversion (decay)

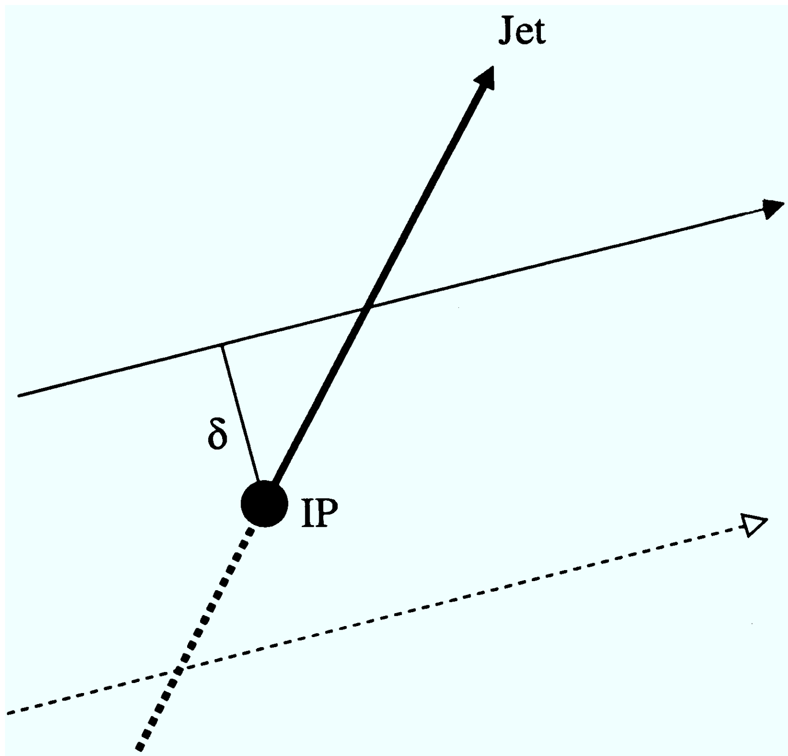

Figure 4.2: The definition of the “lifetime-signed" impact parameter. The impact parameter is the distance of closest approach to the interaction point, and its sign is chosen based on whether it crosses the jet axis upstream (solid track) or downstream (dashed track) of its point of closest approach to interaction point.

Muons	%	Electrons	%
$\Lambda_{\rm b} \to \mu$	$58 \pm 4\%$	$\Lambda_{\rm b} \to e$	$57 \pm 4\%$
$\rm b \to \mu$	$34 \pm 3\%$	$\rm b \to e$	$38 \pm 3\%$
$\rm b \to (c/\tau) \to \mu$	$3.3 \pm 0.3\%$	$\rm b \to (c/\tau) \to e$	$3.3 \pm 0.3\%$
$\rm c \to \mu$	$1.8 \pm 0.2\%$	$\rm c \to e$	$1.7 \pm 0.2\%$
Misidentified hadrons	$1.6 \pm 0.2\%$	Misidentified hadrons	$0.4 \pm 0.1\%$
π and K decays	$1.5 \pm 0.2\%$	γ conversions	$0.1 \pm 0.1\%$

Table 4.1: Monte Carlo lepton sample composition.

The first component is the signal while the remainder are background. Let $f_{\Lambda_{\rm b}}$, f_b, f_{bc}, f_c, f_{miss} and f_{dec} represent the fractions of the above sources of lepton. The fraction of the signal relative to the background is taken from the ratio of $\Lambda\ell^{\perp}$and $\Lambda\ell^{+}$correlations, corrected for the production asymmetry for the accidental Λl pairs. The relative background fractions are taken from Monte Carlo events and a possible disagreement with the data is considered in evaluating the systematic error. The sample composition is shown in Table 4.1.

The impact parameter distribution for prompt lepton sources (first four components) is obtained by convoluting a resolution function with the so-called “physics functions" which describe the expected impact parameter distributions. Reconstructed tracks in the data are used to model the shape of the resolution function, while the physics function is obtained separately for each lepton source from a Monte Carlo simulation of the decay process. Monte Carlo studies have revealed a correlation between the lepton impact parameter and the momentum of the associated Λ candidate, due to kinematic constraints in the event. The requirement of a Λ candidate in the event together with a lepton modifies the lepton impact parameter distribution (Figure 4.3).

Therefore, in contrast to the previous paper [10], the physics functions for the $\Lambda_{\rm b} \to l$ and for the b $\to l$ component are obtained from $\Lambda\ell^{\perp}$ combinations selected in Monte Carlo Z$\to$ $\rm q\overline{q}$ events. The physics function for $\Lambda_{\rm b} \to l$ (i.e. $\mathcal{P}_{\Lambda_{\rm b}}$) is shown in Figure 4.4.

Moreover, two different physics functions (Figure 4.5) are used for the underlying of the b $\to l$ (i.e. $\mathcal{P}_{\rm b}$) background, according to the source of the associated Λ candidate:

- b $\to l$ with an accidental Λ, i.e. a Λ coming from fragmentation;
- b $\to l$ with a fake p$\pi^{\perp}$ combination.

The difference of the physics functions is due to the different momentum spectra of the Λ candidates in the two cases.

Two separate physics functions are used for these two sources of backgrounds because the shapes of the physics functions are significantly different, largely due to kinematic reasons. When a fragmentation Λ is present in the event, the b hadron spectrum is pushed towards lower values in order to conserve the total momentum. A lower b momentum means a smaller impact parameter. On the other hand, as the two tracks which give the fake Λ mainly come from the b decay, the resulting lepton spectrum is softer, as the Λ must take at least 3 GeV/c in order to be selected. For the P and $P_{\perp}$ cuts applied to the lepton, a softer spectrum results in a larger

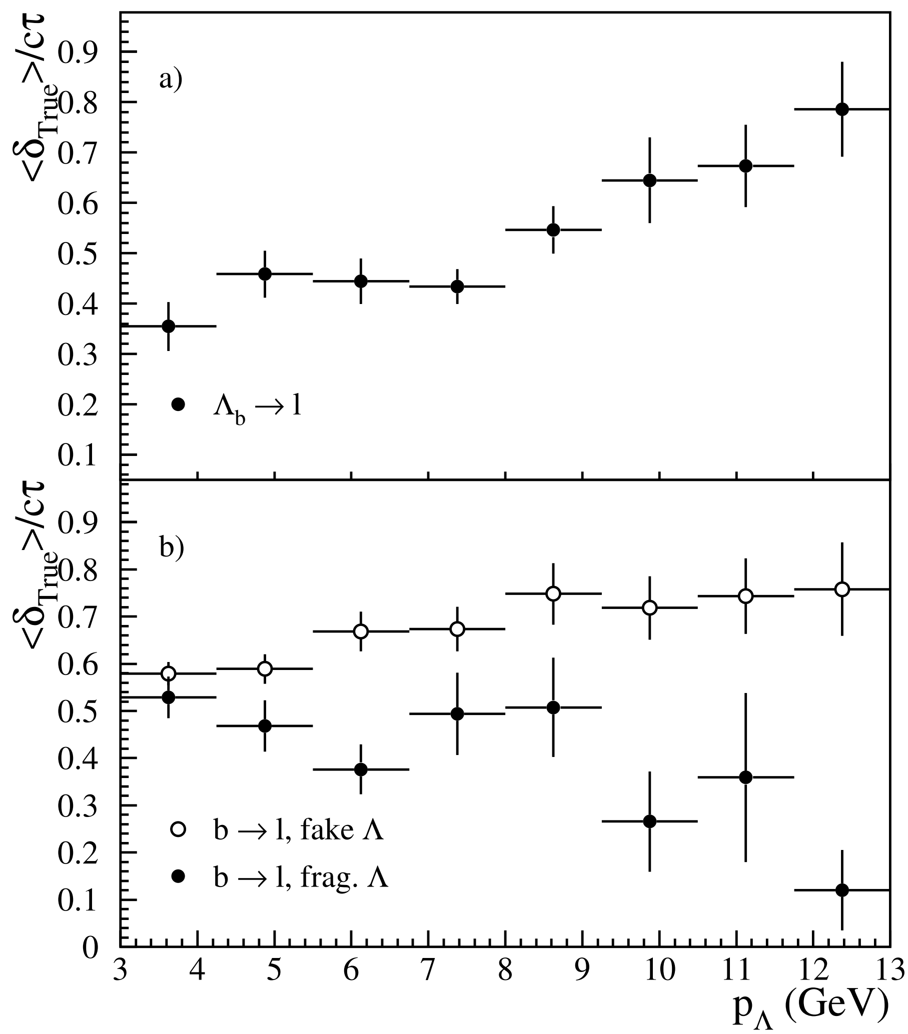

Figure 4.3: Average value of the expected impact parameter, divided by $c\tau$, for leptons from semileptonic decay of Λ_b (a) and for leptons from generic b decays which are associated with fragmentation or combinatorial (fake) Λ (b).

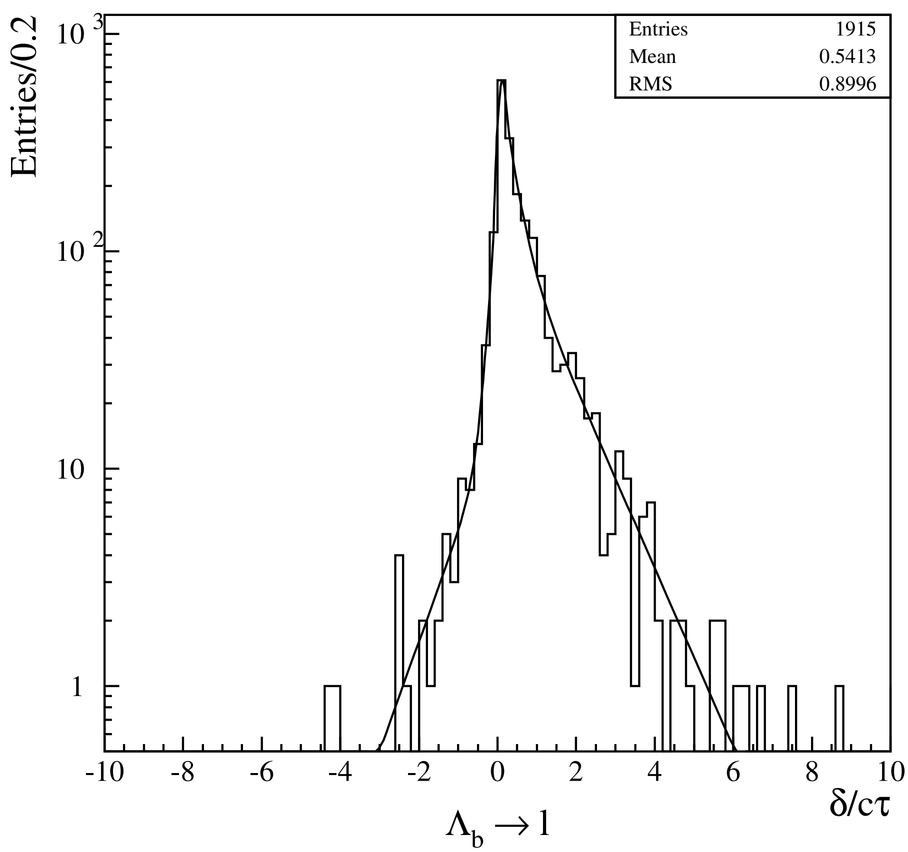

Figure 4.4: Physics function for leptons coming directly from Λ_b semileptonic decay. The negative tail is due to the error in the reconstruction of the jet direction which is used to sign the impact parameter.

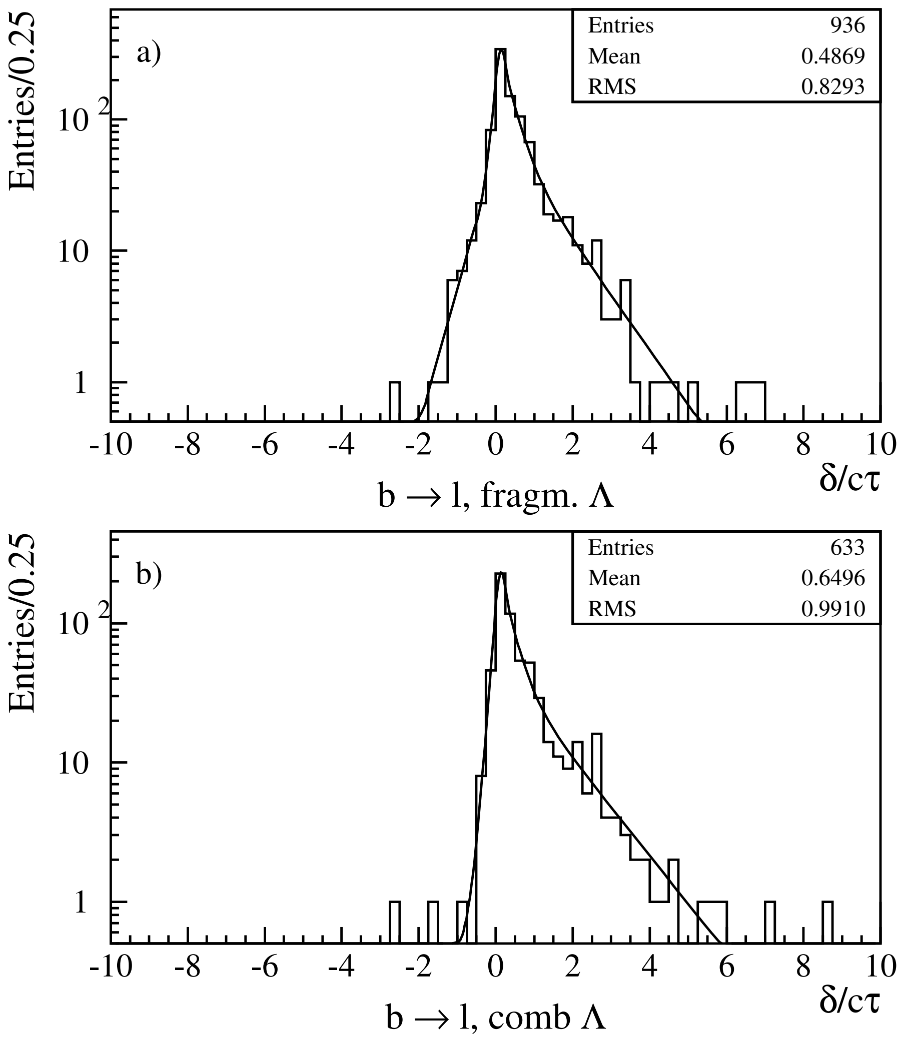

Figure 4.5: Physics functions for b $\rightarrow$ l associated with a Λ from fragmentation (a) and a fake Λ (b).

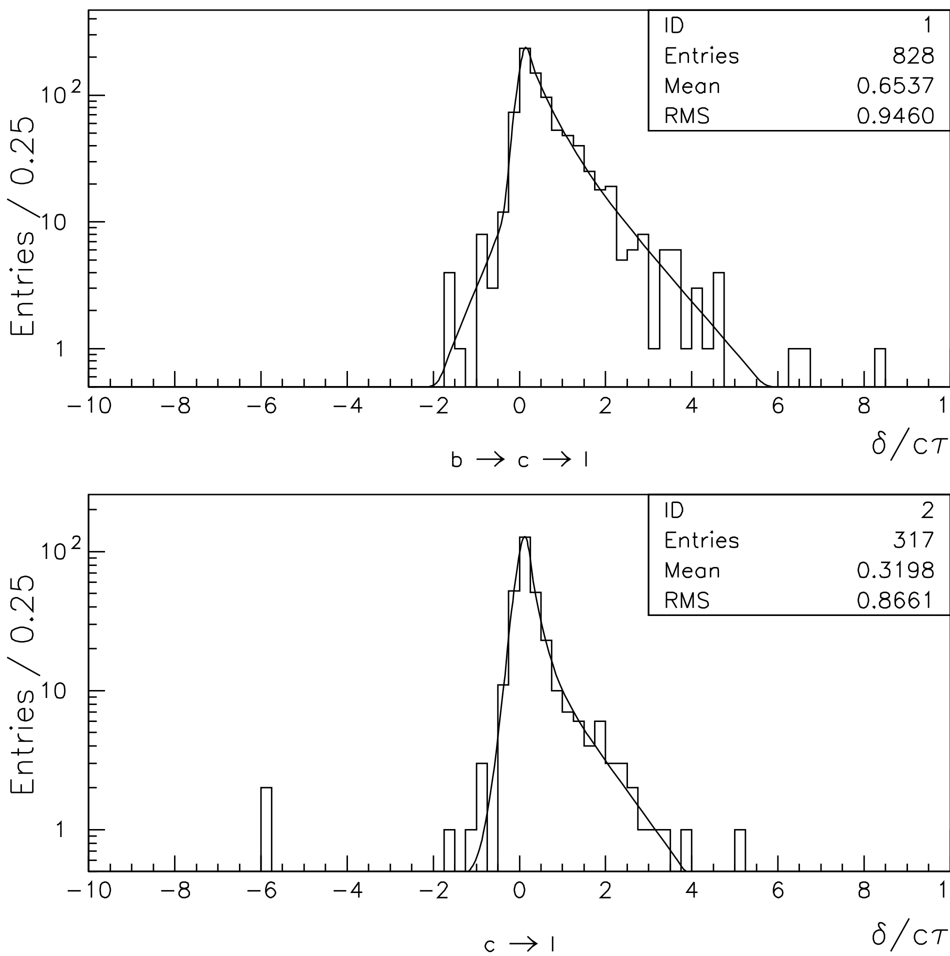

Figure 4.6: Physics functions for b $\rightarrow$ c $\rightarrow$ l and c $\rightarrow$ l.

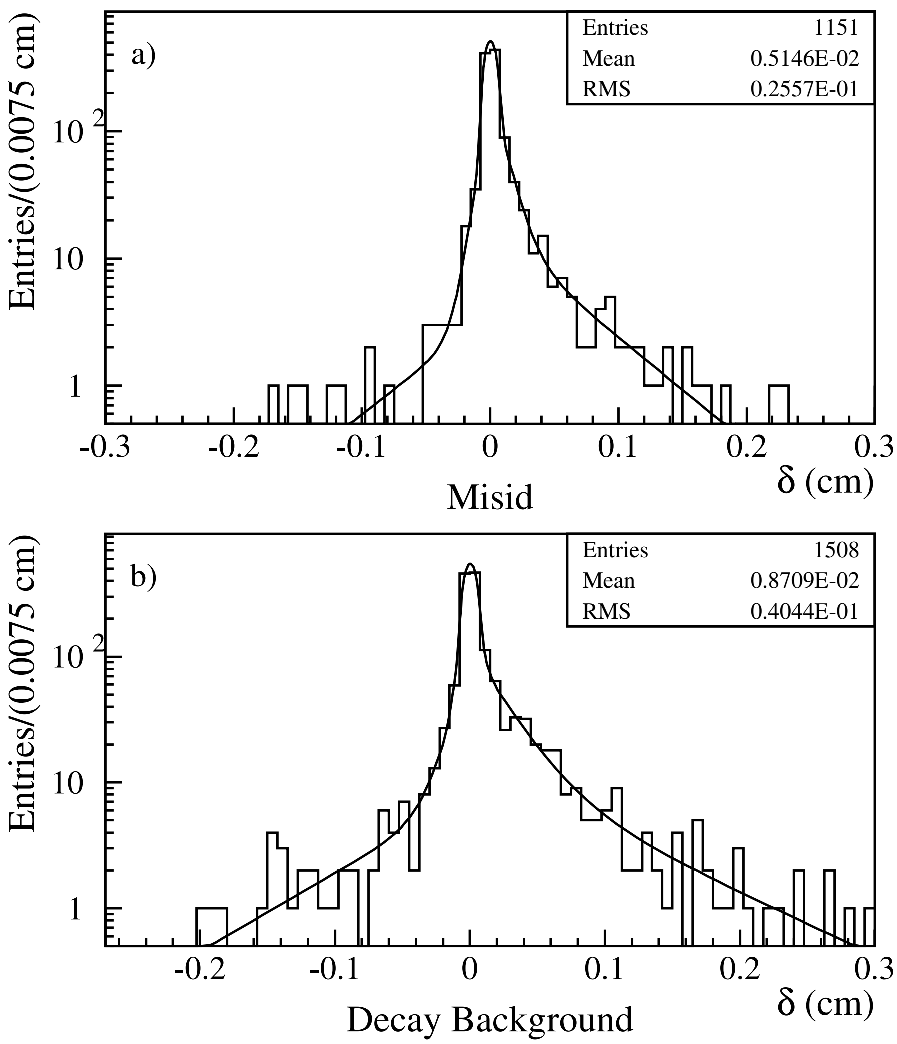

Figure 4.7: Impact parameter distributions for misidentified hadrons (a) and non-prompt leptons (b).

decay angle and consequently a larger impact parameter. As can be seen in Figure 4.5, the functions are clearly different and this difference increases as the cut in the Λ momentum is raised because of the two kinematic effects described. In Figure 4.3 the average values of the impact parameter as a function of the associated Λ momentum for the signal and the two different b $\rightarrow$ l background sources are shown. The relative fraction of the two b $\rightarrow$ l components is measured from the ratio obtained in the simulated events. However, it is in agreement with the result of the Λ invariant mass fit in the data for the $\Lambda l^{\perp}$ and Λl^{+} samples.

The expected impact parameter distribution for b $\rightarrow$ c $\rightarrow$ l and c $\rightarrow$ l are obtained similarly from Monte Carlo simulation and the physics functions for these two processes (i.e. $\mathcal{P}_{\rm bc}$ and $\mathcal{P}_{\rm c}$) are shown in Figure 4.6.

The expected impact parameter distribution for the hadron misidentification (i.e. $\mathcal{P}_{miss}$) is obtained directly from the impact parameter distribution of hadrons selected in the data with the same kinematic cuts as the leptons. In addition the presence of an identified Λ is required in the event. The distribution for the leptons coming from decay in flight of K and π (i.e. $\mathcal{P}_{dec}$) is taken directly from the simulated events. Physics functions for these two processes are shown in Figure 4.7.

4.3 Impact Parameter Resolution Function

Errors in the measurement of the impact parameter of a given track come from sources like intrinsic resolution of tracking detectors, multiple scattering in detector material and interaction point estimation etc.

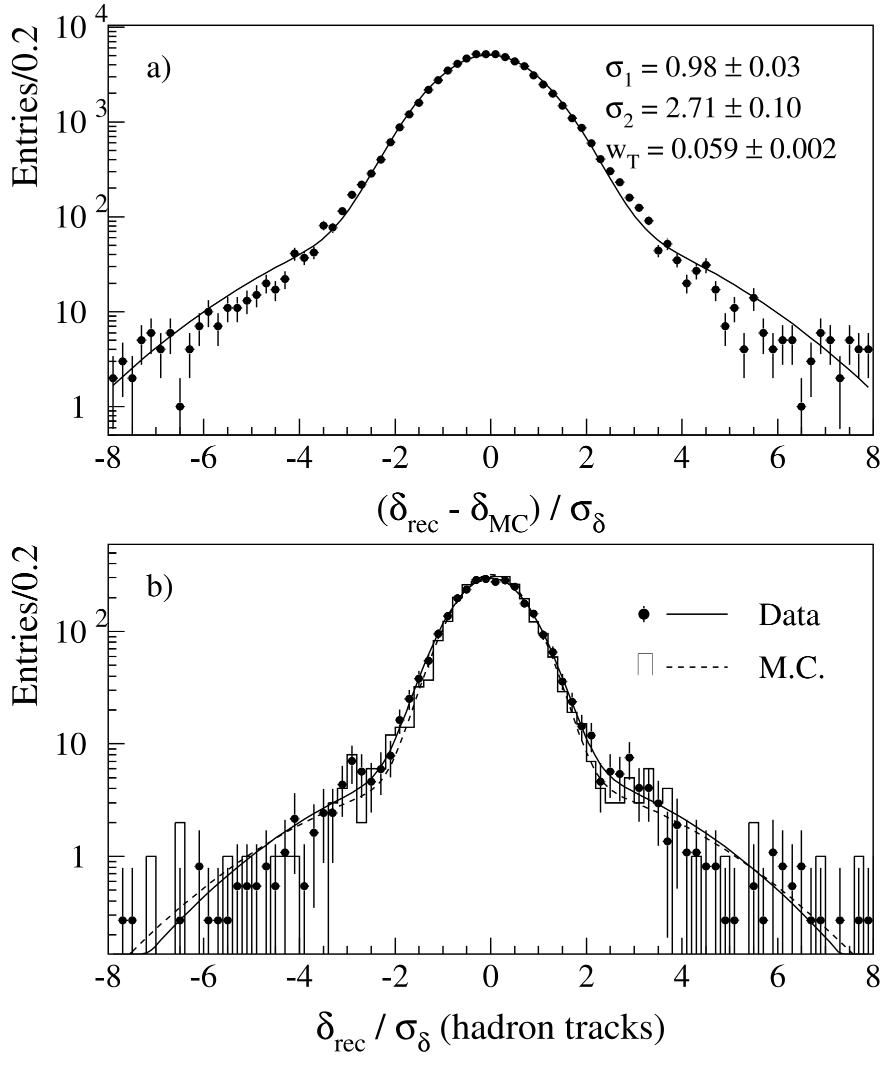

Figure 4.8: a) Resolution function for leptons selected in Monte Carlo events. b) Impact parameter distribution of hadron tracks selected in uds events in data (solid line) and Monte Carlo (dashed line). Only the tracks which have a negative impact parameter are displayed with a random sign in order to help the fit.

The resolution function is obtained using Monte Carlo events by plotting the difference between the reconstructed and the true impact parameter over the measured error for the selected lepton tracks, as shown in Figure 4.8. In addition, a correction factor is applied to the resolution function in order to take into account the difference in the tracking resolution between data and Monte Carlo. This correction is obtained by comparing the negatively signed part of the impact parameter distribution of hadron tracks in data and Monte Carlo samples of enriched light quark events. The hadron tracks are selected with the same quality and kinematic cuts as for the lepton candidates except for the lepton identification requirement. All the tracks in Z$\rightarrow$ $\mathrm{u\overline{u}, d\overline{d}, s\overline{s}}$ events come from the primary vertex and they have a random signed impact parameter, while tracks coming from a secondary vertex or from long-lived particles usually have a positive impact parameter. Therefore the measured impact parameter with a negative sign contains only resolution effects. The Z$\rightarrow$ $\mathrm{u\overline{u}, d\overline{d}, s\overline{s}}$ events are isolated using a Z$\rightarrow$ $\mathrm{b\overline{b}}$ event tagging technique on the hemisphere opposite to the hadron track [40].

4.4 b Baryon Lifetime Fit

The likelihood function $\mathcal{L}$ to be maximised is built up as the product of the total probability density functions for all the N lepton candidates:

$$\mathcal{L} = \prod_{i=1}^{N} (f_{\Lambda_\mathrm{b}} \mathcal{P}_{\Lambda_\mathrm{b}}(\tau_{\Lambda_\mathrm{b}}, \delta_i, \sigma_i) + f_\mathrm{b} \mathcal{P}_\mathrm{b}(\tau_\mathrm{b}, \delta_i, \sigma_i) + f_\mathrm{bc} \mathcal{P}_\mathrm{bc}(\tau_\mathrm{b}, \delta_i, \sigma_i) \\ + f_\mathrm{c} \mathcal{P}_\mathrm{c}(\tau_\mathrm{c}, \delta_i, \sigma_i) + f_{miss} \mathcal{P}_{miss}(\delta_i) + f_{dec} \mathcal{P}_{dec}(\delta_i))$$

where δ_i is the impact parameter of the i-th lepton candidate and σ_i is the related error. f_{Λ_b}, f_b, f_{bc}, f_c, f_{miss} and f_{dec} are the fractions of the possible sources of lepton in the $\Lambda l^{\perp}$ sample as shown in Table 4.1. $\mathcal{P}_{\Lambda_\mathrm{b}}$, $\mathcal{P}_\mathrm{b}$, $\mathcal{P}_\mathrm{bc}$, $\mathcal{P}_\mathrm{c}$, $\mathcal{P}_{miss}$, $\mathcal{P}_{dec}$ are the normalized physics functions for those lepton sources as described in the previous section, convoluted with the resolution function. The b baryon lifetime $\tau_{\Lambda_\mathrm{b}}$ is the only free parameter of the fit.

The signal physics function depends on the unknown Λ_b lifetime, while the b $\rightarrow$ l and b $\rightarrow$ c $\rightarrow$ l background physics functions depend on the inclusive b hadron lifetime. The value used in the fit is a world average of all the b lifetime measurements, $\tau_\mathrm{b} = 1.537 \pm 0.021$ ps [5].

The maximum likelihood fit to the impact parameter distribution of the lepton candidates in the 519 $\Lambda l^{\perp}$ candidates yields a b baryon lifetime:

$$\tau_{\Lambda_\mathrm{b}} = 1.05\,^{+0.12}_{-0.11}\ \mathrm{ps}$$

where the above error is the statistical one coming from the fit. Figure 4.9 shows the result of fit together with the observed impact parameter distribution of the lepton candidates in the $\Lambda\ell^{\perp}$sample.

4.5 Systematic Checks

Several checks have been performed in order to look for possible systematic effects which could affect the fitted b baryon lifetime value. First, in order to check the

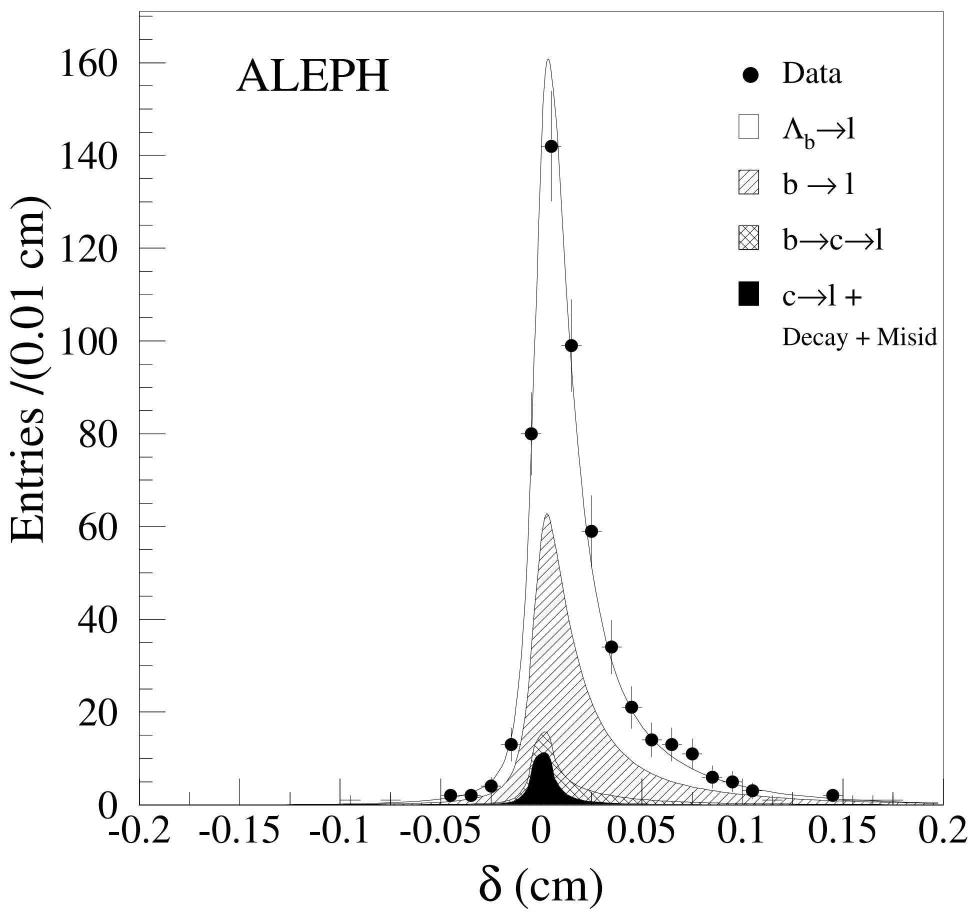

Figure 4.9: Impact parameter distribution of the selected $\Lambda l^{\perp}$ candidates. The solid line is the probability function at the fitted value of the lifetime.

fitting procedure, the analysis has been applied to a Monte Carlo sample of about 3,000,000 equivalent $\mathrm{q\bar{q}}$ events generated with an input Λ_b lifetime of 1.5 ps. From 987 $\Lambda l^{\perp}$ and 569 Λl^{+} selected events, the fit yields a result of $\tau_{\Lambda_\mathrm{b}} = 1.48 \pm 0.13$ which is consistent with the input value of 1.50 ps.

A further check is performed repeating the fit on various samples of data selected with different cuts. The lepton kinematic cuts on P and $P_{\perp}$ and the Λ momentum are varied. A deviation from the standard value is observed only when increasing the minimum Λ momentum from 3 GeV/c up to 7 GeV/c. The fitted lifetime values obtained with different lepton P, $P_{\perp}$ and Λ momentum cuts are shown in Figure 4.10 and 4.11. The errors shown are the uncorrelated statistic and systematic error with respect to the standard value. However it is not possible, from the observed deviation, to conclude whether a systematic effect is present. Moreover the same check applied to the $\Lambda l^{\perp}$ sample of Monte Carlo events which is approximately a factor of two larger, gives a very stable result (Figure 4.12).

The background physics functions are checked by fitting the events in the side bands of the p$\pi^{\perp}$ invariant mass for a measurement of the inclusive b lifetime. The relative fractions of the different sources of the inclusive leptons which are taken from the inclusive b lifetime analysis are checked together with the background physics functions. For the b $\rightarrow$ l part, only the component associated with a fake Λ is used in the fit. The fit yields a result of τ_b(side bands) $= 1.52 \pm 0.07$ ps which is in good agreement with the inclusive b hadron lifetime value [5].

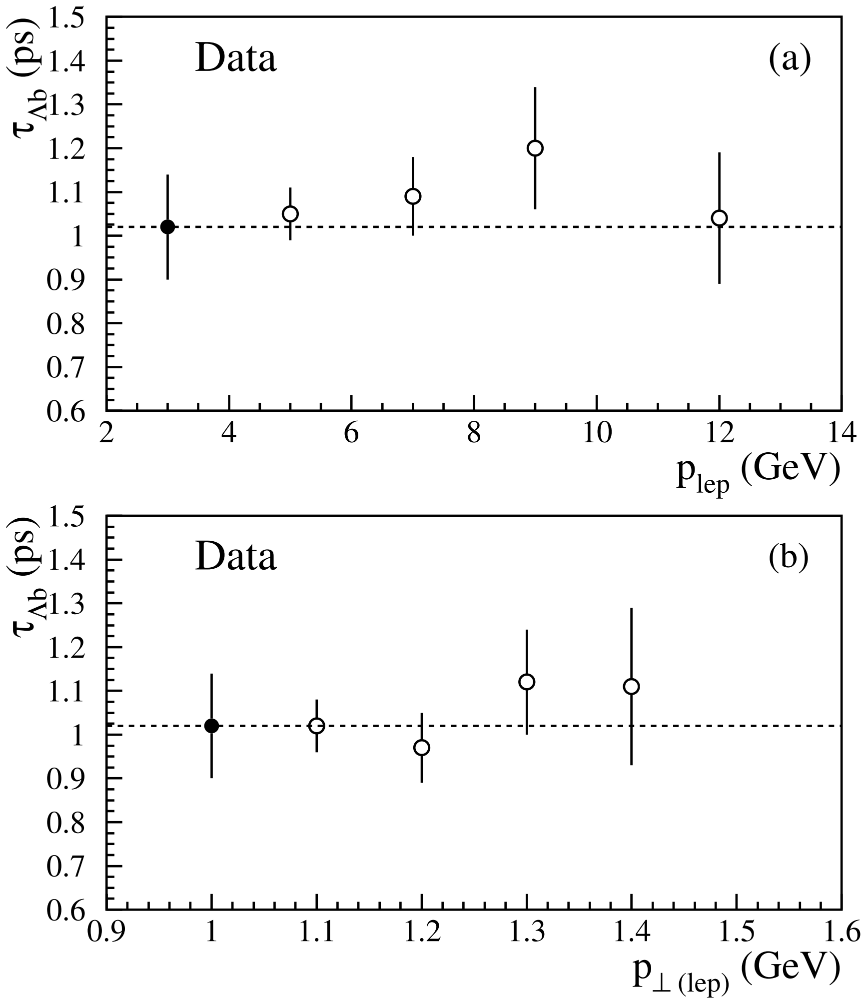

Figure 4.10: Lifetime of the b baryon in the data as function of the momentum of the lepton (a) and the transverse momentum of the lepton (b). The error at the solid dot is statistical while the increases of error with respect to this solid dot are shown at other open points.

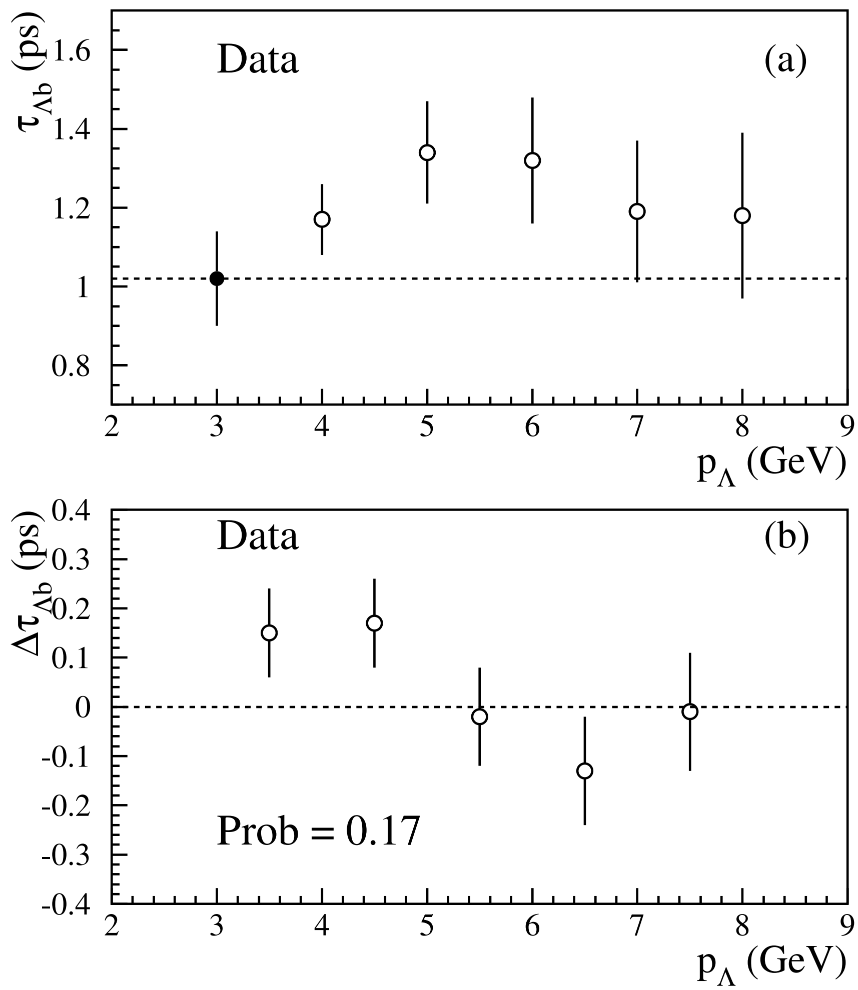

Figure 4.11: (a) Lifetime of the b baryon as function of the Λ momentum cut for the data. The error at the solid dot is statistical while the increases of error with respect to this solid dot are shown at open points. (b) Difference between two consecutive lifetime values obtained for various Λ momentum cuts with the difference of the errors. The points have a spread with respect to zero (dashed line) of a χ^2 probability of 17%, indicating that this variation is not very significant.

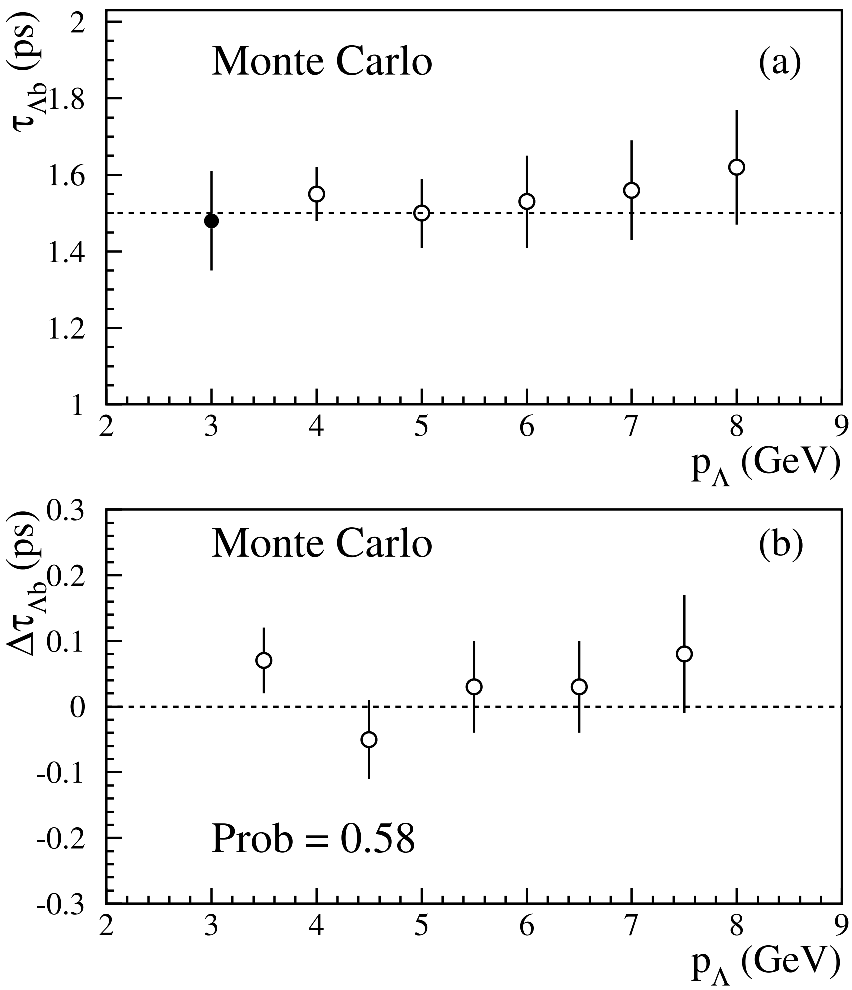

Figure 4.12: (a) Lifetime of the b baryon as function of the Λ momentum cut for the Monte Carlo. The error at the solid dot is statistical while uncorrelated statistical errors with respect to this solid dot are shown on open points. (b) Difference between two consecutive lifetime values obtained for various Λ momentum cuts with the uncorrelated error. The points have a spread with respect to zero (dashed line) of a χ^2 probability of 58%.

Source of systematic error	Uncertainty (ps)
b baryon fraction ($f_{\Lambda_b} = 58 \pm 10\%$)	${}^{+0.04}_{\perp 0.05}$
Background lepton fractions	± 0.03
Effective background lifetime ($\tau_b = 1.537^{+0.054}_{\perp 0.021}$ ps)	${}^{+0.01}_{\perp 0.03}$
$\Lambda_b \to \ell$ physics function	± 0.03
Background physics functions	± 0.03
Λ_b polarisation ($\mathcal{P}_{\Lambda_b} = \perp 30^{+32}_{\perp 27}\%$)	± 0.03
Λ_b decay model (4-body decay $20 \pm 20\%$)	± 0.02
Fragmentation ($\langle x_b \rangle = 0.714 \pm 0.012$)	± 0.02
Fragmentation Λ spectrum ($\pm 10\%$)	± 0.02
Decay background and Misid function	± 0.02
Resolution function	± 0.02
Level of combinatorial Λ ($\pm 15\%$)	± 0.01
Total	± 0.09

Table 4.2: Contributions to the systematic uncertainty in the b baryon lifetime measurement using $\Lambda\ell^{\perp}$ sample.

4.6 Systematic Errors

In Table 4.2, the various contributions to the systematic uncertainty in the b baryon lifetime measurement are listed in order of importance. The major contribution to the systematic error is from the uncertainty in the b baryon fraction (58 $\pm$ 10%). This uncertainty is dominated by the error in the estimate of the number of accidental combinations of $\Lambda\ell^{\perp}$ with respect to $\Lambda\ell^{+}$. The value for the ratio of accidental $\Lambda\ell^{\perp}$ over the $\Lambda\ell^{+}$ combinations used, 0.8 ± 0.2 , contributes an error of ${}^{+0.04}_{\perp 0.05}$ ps to the b baryon lifetime.

The relative fractions of the various background sources are obtained from a Monte Carlo simulation and their uncertainty leads to a systematic contribution of ± 0.03 ps to the b baryon lifetime.

The physics functions depend on the average lifetimes of the b and c hadrons which populate the right-sign ($\Lambda\ell^{\perp}$) peak. The assumption that these have the same b hadron composition in $\mathrm{b} \rightarrow \ell$ sample as that used in measurements of the average b hadron lifetime [5] is also considered as a source of systematic error. Simulation studies based on JETSET 7.3 program have shown that the b baryon production is suppressed in events where a lepton is associated with a right-sign accidental Λ. This is the same effect which creates the asymmetry in the $\Lambda\ell^{\perp} \perp \Lambda\ell^{+}$ accidental combinations. A variation in the effective background lifetime of $^{+0.054}_{\perp 0.021}$ ps which includes the full suppression of b baryon yields a systematic error of $^{+0.01}_{\perp 0.03}$ ps on the b baryon lifetime. The error on the average c lifetime has a negligible effect, due to the low charm background.

Another source of systematic uncertainty arises from the limited sample of simulated events used to parametrise the physics functions. The statistical uncertainties in the parameters of each physics function leads to an estimated error on b baryon lifetime of ± 0.03 ps for the $\Lambda_{\mathrm{b}} \rightarrow \ell$ function and ± 0.03 ps for the $\mathrm{b} \rightarrow \ell$, $\mathrm{b} \rightarrow \mathrm{c}/\tau \rightarrow \ell$ and $\mathrm{c} \rightarrow \ell$ combined.

An important systematic uncertainty arises from the lack of knowledge of the Λ_{b} polarisation. The $\Lambda_{\mathrm{b}} \rightarrow \ell$ physics function is sensitive to the polarisation of the Λ_{b}, because the impact parameter of the lepton is correlated with its decay angle. In Z$\rightarrow \mathrm{b}\overline{\mathrm{b}}$ decays, the b quark is produced with a longitudinal polarisation of $\perp 94\%$ [41, 35]. b baryons can retain some fraction of this primordial polarisation.

If the $\Lambda_{\rm b}$ is longitudinally polarised, the resulting lepton is produced preferentially along the $\Lambda_{\rm b}$ direction and oppositely to the polarisation vector. Therefore, due to the $\Lambda_{\rm b}$ boost, a left-hand polarisation of the $\Lambda_{\rm b}$ results, for the same lifetime, in a harder lepton spectrum and a smaller lepton impact parameter than if $\Lambda_{\rm b}$ were unpolarised. Figure 4.13 shows the expected spectrum as function of $x = E_l/E_{\Lambda_{\rm b}}$ for polarized and unpolarized semileptonic decays of b quarks.

The uncertainty in the knowledge of the $\Lambda_{\rm b}$ polarisation ($\mathcal{P}_{\Lambda_{\rm b}} = \perp 30^{+32}_{\perp 27}\%$) [38], used in this analysis, leads to a systematic error of ± 0.03 ps.

A variation in the 4-body semileptonic b hadron decay rate (relative to the total b hadron semileptonic decay rate) of $\pm 20\%$ leads to a change of ± 0.02 ps in the b baryon lifetime. Uncertainties in the rate of different exclusive decay modes which make up the inclusive $\Lambda_{\rm c}^{+} \rightarrow \Lambda{\rm X}$ rate gives a negligible contribution.

A further source of systematic error is due to the b fragmentation. A variation of Peterson fragmentation function which covers the uncertainty in the measurement of b hadron momentum ($\langle x_{\rm b} \rangle = 0.714 \pm 0.012$) [42] leads to a ± 0.02 ps variation in the b baryon lifetime.

The shape of the ${\rm b} \rightarrow \ell$ physics function is different for true Λ's produced during fragmentation and the combinatorial ${\rm p}\pi^{\perp}$ combinations. In particular, a change in the Λ momentum spectrum would affect the shape of the physics function. Therefore a further uncertainty arises in the simulation of the hadronization process which produces fragmentation Λ's. The momentum spectrum of Λ's produced in hadronic events simulated with the JETSET 7.3 has been compared with the data [43] and shows a good agreement. However, an uncertainty of 10% in the shape of the fragmentation Λ momentum spectrum is assumed, leading to an

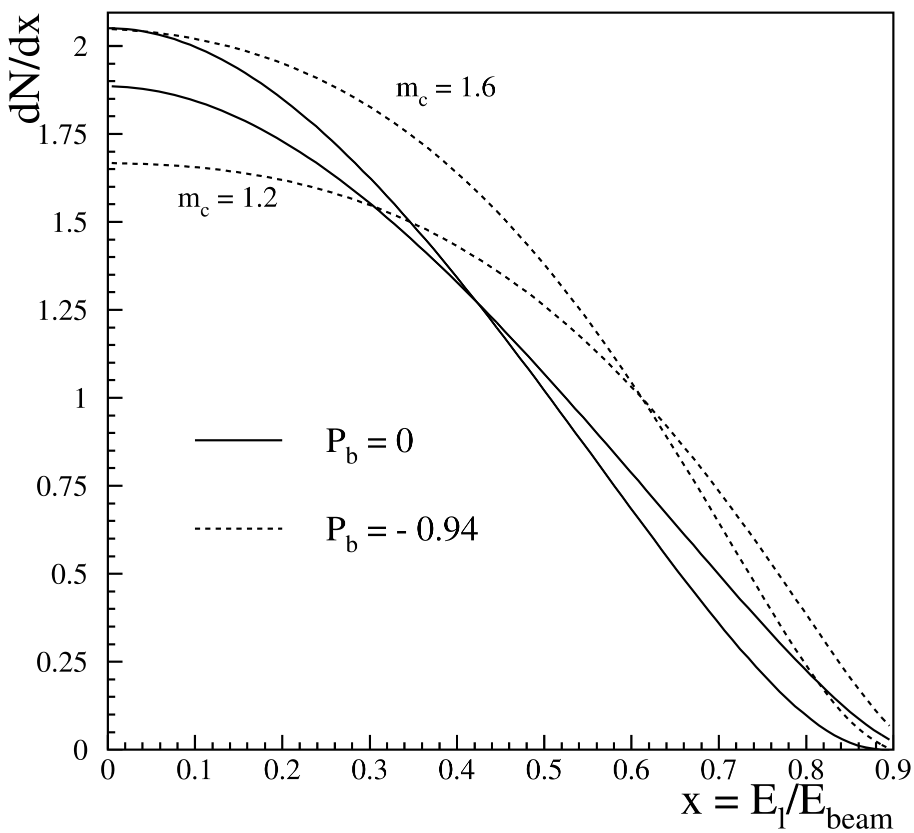

Figure 4.13: Lepton spectrum in the laboratory frame for a 100% left hand polarization ($P_{\mathrm{b}} = \perp 0.94$, dashed lines) compare to the unpolarized case ($P_{\mathrm{b}} = 0$, solid lines) for different values of m_{c}. Fragmentation effects are not included ($E_{\mathrm{b}} \equiv E_{beam}$).

error of 0.02 ps in the lifetime measurement.

The statistical error in the parametrisation of the misidentification and decay background probability function is negligible. Nevertheless an error of 0.02 ps is assigned to include possible uncertainties in the simulation of the decay background events used to derive the expected shape of the function.

The statistical error on the parametrisation of the resolution function gives a negligible uncertainty to the b baryon lifetime measurement. An error of 0.02 ps is estimated from the variation in b baryon lifetime when the uncorrected resolution function estimated using simulated events is replaced by the functional form corrected using data.

The number of combinatorial Λ is obtained by interpolating the polynomial fit of the $\mathrm{p}\pi^{\perp}$ invariant mass from the side bands to the region under the peak. A fit uncertainty of 15% results in a systematic contribution of ± 0.01 ps.

Summing all the systematic contributions in quadrature yields a total systematic error on the b baryon lifetime of ± 0.09 ps.

Chapter 5

Conclusion and Outlook

5.1 Conclusion

From a total of about 1,500,000 hadronic Z decays collected with the ALEPH detector during the 1991, 1992 and 1993 data taking periods, when the silicon vertex detector was fully operational, the yields of $\Lambda\ell^{\perp}$ and $\Lambda\ell^{+}$ combinations are measured. Semileptonic decays of b baryons result in a signal of $290 \pm 35(\mathrm{stat}) \pm 39(\mathrm{syst})$ $\Lambda\ell^{\perp}$ combinations from b baryon decays, which corresponds to a product branching ratio:

$$\mathrm{Br}(\mathrm{b} \to \Lambda_{\mathrm{b}}) \cdot \mathrm{Br}(\Lambda_{\mathrm{b}} \to \Lambda_{\mathrm{c}}^{+}\ell^{\perp}\overline{\nu}X) \cdot \mathrm{Br}(\Lambda_{\mathrm{c}}^{+} \to \Lambda X)$$

$$= (0.61 \pm 0.07(\mathrm{stat}) \pm 0.10(\mathrm{syst}))\%$$

The lifetime of b baryons is extracted from a maximum likelihood fit to the impact parameter distribution of the candidate lepton tracks of the $\Lambda l^{\perp}$ sample. The result is:

$$\tau_{\Lambda_b} = 1.05\,^{+\,0.12}_{-\,0.11}\,\text{(stat)} \pm 0.09\,\text{(syst) ps}$$

This value can be compared with the LEP average of the B^0 lifetime of 1.56 ± 0.07 ps [44]. Figure 5.1 shows the comparison of Λ_b lifetime with B^0 lifetime. It can be seen that they are considerably different with each other. The ratio of the lifetimes of Λ_b and B^0 hadrons is 0.67 ± 0.09, which is substantially smaller than the theoretical estimate of 0.9 [7].

This difference between the experimental measurement and the theoretical prediction remains to be understood. More work, both theoretical and experimental, is needed to understand the decay of b hadrons, especially the decay of b baryons.

5.2 b Baryon Lifetime Measurement Using $\Lambda_c^+\ell^-$ Correlation in ALEPH

Besides the b baryon lifetime measurement using $\Lambda\ell^-$ correlation described in this dissertation, b baryon lifetime was also measured using $\Lambda_c^+\ell^-$ correlation with the exclusive reconstruction of Λ_c^+ in ALEPH. The $\Lambda_c^+\ell^-$ combinations allow measurement of the Λ_b decay vertex and hence its decay length on an event-by-event basis. Although statistically less powerful for Λ_b identification compared with the $\Lambda\ell^-$ method, this decay channel gives an independent Λ_b sample and has

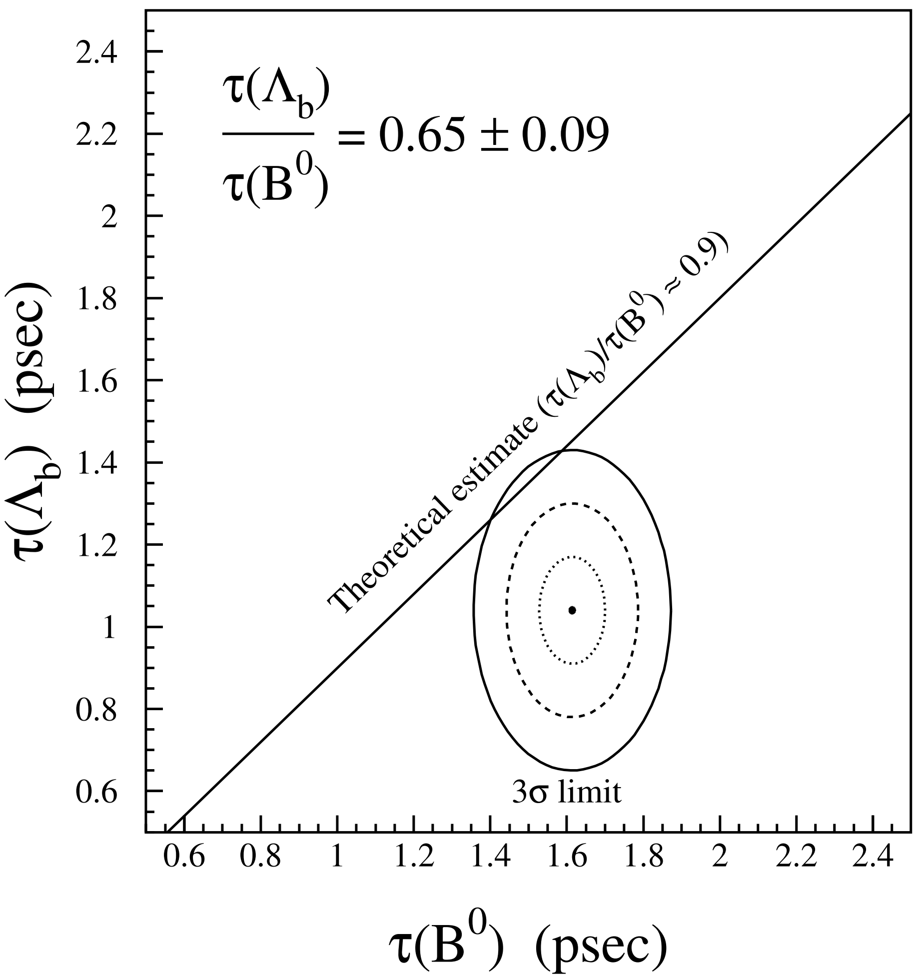

Figure 5.1: Comparison of Λ_b lifetime with B^0 lifetime.

the advantage of being insensitive to other b baryons [1].

Candidates for the decay $\Lambda_{\mathrm{b}} \rightarrow \Lambda_{\mathrm{c}}^{+}\ell^{\perp}\overline{\nu}$ are identified in hadronic Z events where a Λ_{c}^{+} is associated with a lepton in the same hemisphere with respect to the thrust axis. The Λ_{c}^{+} candidates are reconstructed in three decay modes, namely, $\Lambda_{\mathrm{c}}^{+} \rightarrow \mathrm{pK}^{\perp}\pi^{+}$, $\Lambda_{\mathrm{c}}^{+} \rightarrow \Lambda\pi^{+}\pi^{+}\pi^{\perp}$ and $\Lambda_{\mathrm{c}}^{+} \rightarrow \mathrm{p}\bar{\mathrm{K}}^{0}$. Measurement of Λ_{b} lifetime using $\Lambda_{\mathrm{c}}^{+}\ell^{\perp}$ where $\Lambda_{\mathrm{c}}^{+} \rightarrow \mathrm{pK}^{\perp}\pi^{+}$ was done by Vivek Sharma, Min Zheng of Wisconsin group together with Mossadek Talby, Delphine Nicod of Marseille group while measurement using the two other $\Lambda_{\mathrm{c}}^{+} \rightarrow \Lambda\pi^{+}\pi^{+}\pi^{\perp}$ and $\Lambda_{\mathrm{c}}^{+} \rightarrow \mathrm{p}\bar{\mathrm{K}}^{0}$ decay modes was done by Paolo Spagnolo of Pisa group.

Figure 5.2 shows the individual contributions of the three Λ_{c}^{+} decay channels to the right-sign $\Lambda_{\mathrm{c}}^{+}\ell^{\perp}$ combinations and their sum after all cuts. A clear enhancement is observed at the nominal Λ_{c}^{+} mass value in the right-sign $\Lambda_{\mathrm{c}}^{+}\ell^{\perp}$ combinations (Figure 5.2(d)) while for wrong-sign $\Lambda_{\mathrm{c}}^{+}\ell^{+}$ events (Figure 5.2(e)) no such enhancement is observed. Table 5.1 summarises the number of $\Lambda_{\mathrm{c}}^{+}\ell^{\perp}$ candidates selected in the three Λ_{c}^{+} decay channels.

The Λ_{b} lifetime is extracted from a simultaneous unbinned maximum likelihood fit to the proper time distribution of the three $\Lambda_{\mathrm{c}}^{+}\ell^{\perp}$ event samples. The event samples used to extract the Λ_{b} lifetime are shown in Table 5.1. The total sample consists of N_{peak} $\Lambda_{\mathrm{c}}^{+}\ell^{\perp}$ events, in which a fraction f_{back} is attributed to combinatorial background events. To determine the background parametrisation for each $\Lambda_{\mathrm{c}}^{+}\ell^{\perp}$ event sample, right-sign events from side bands more than 4σ outside the nominal Λ_{c}^{+} mass and wrong-sign events (N_{back}) are included in the fit. Figure

[1] Semileptonic decays of other b baryons (for example, Ξ_{b}) involve, besides the lepton, mainly strange-charmed baryons in the final state.

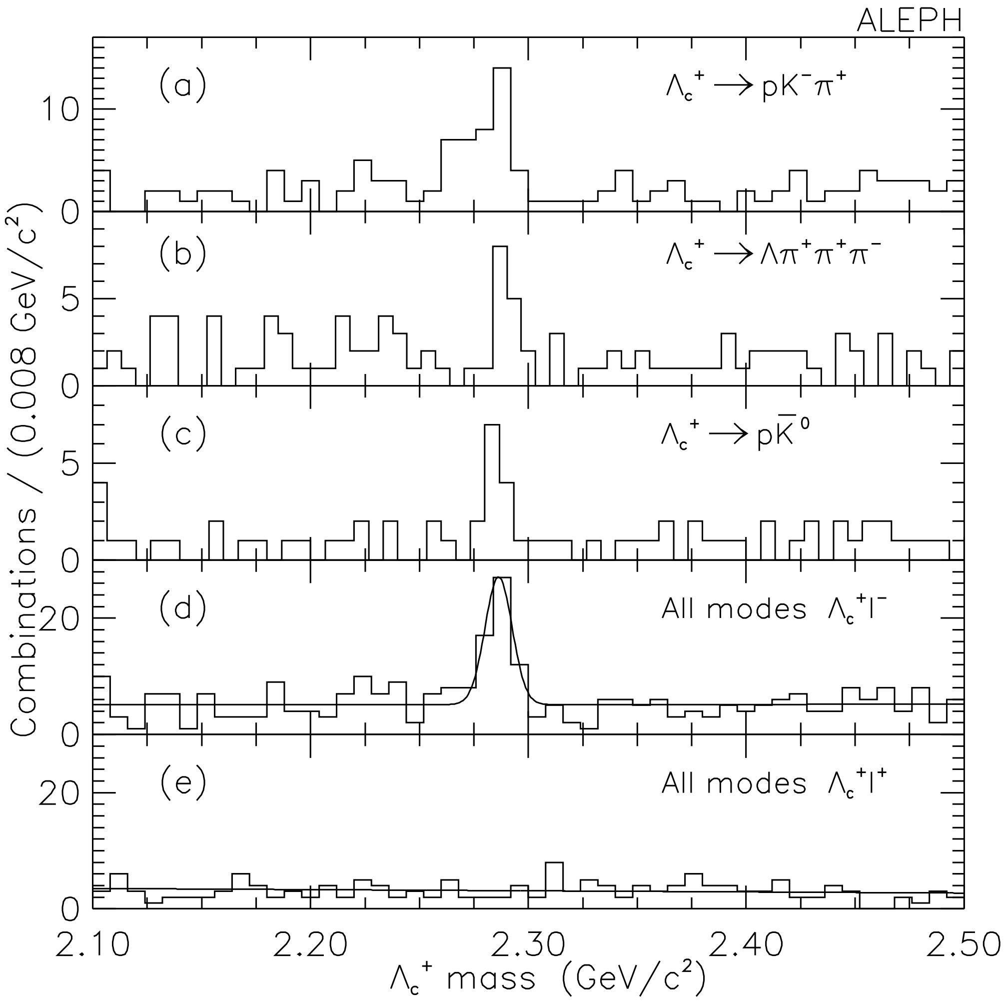

Figure 5.2: The $\mathrm{pK}^{\perp}\pi^{+}$ (a), the $\Lambda\pi^{+}\pi^{+}\pi^{\perp}$ (b), and the $\mathrm{p}\bar{\mathrm{K}}^{0}$ (c) invariant mass distributions for right-sign $\Lambda_{\mathrm{c}}^{+}\ell^{\perp}$ combinations and their sum (d). The sum of wrong-sign $\Lambda_{\mathrm{c}}^{+}\ell^{+}$ combinations is displayed in (e).

Decay Channel	N_{peak}	$f_{back}(\%)$	Mass Resolution (MeV/c^2)
$\Lambda_c^+ \rightarrow \mathrm{pK}^{\perp}\pi^+$	31	23 ± 3	6.9 ± 0.4
$\Lambda_c^+ \rightarrow \Lambda\pi^+\pi^+\pi^{\perp}$	13	24 ± 5	5.3 ± 0.4
$\Lambda_c^+ \rightarrow \mathrm{p}\bar{\mathrm{K}}^0$	14	25 ± 4	8.4 ± 0.3
Total	58	$\perp$	$\perp$

Table 5.1: The number of $\Lambda_c^+\ell^{\perp}$ candidates N_{peak} and the fraction f_{back} of combinatorial background within $\pm 2\sigma$ of the nominal Λ_c^+ mass in the three Λ_c^+ decay modes after all requirements. The invariant mass resolution for each decay mode is also indicated.

5.3 shows the result of the simultaneous fit of the Λ_b signal and combinatorial background events. The fitted Λ_b lifetime is

$$\tau_{\Lambda_\mathrm{b}} \quad = \quad 1.02 \ ^{+0.23}_{\perp 0.18} \ \mathrm{ps}$$

where the quoted error is statistical.

Various sources of systematic uncertainties in $\tau_{\Lambda_\mathrm{b}}$ measurement and their contributions are summarised in Table 5.2.

In summary, $\Lambda_c^+\ell^{\perp}$ combinations from semileptonic decay of the Λ_b are identified via fully reconstructed $\Lambda_c^+ \rightarrow \mathrm{pK}^{\perp}\pi^+$, $\Lambda_c^+ \rightarrow \Lambda\pi^+\pi^+\pi^{\perp}$, and $\Lambda_c^+ \rightarrow \mathrm{p}\bar{\mathrm{K}}^0$ decays. The average product branching ratio is:

$$Br(\mathrm{b} \rightarrow \Lambda_\mathrm{b}) \cdot Br(\Lambda_\mathrm{b} \rightarrow \Lambda_c^+\ell^{\perp}\overline{\nu}\mathrm{X}) = (1.51 \pm 0.29(\mathrm{stat}) \pm 0.23(\mathrm{syst}))\%$$

The Λ_b lifetime measured from a maximum likelihood fit of the proper decay

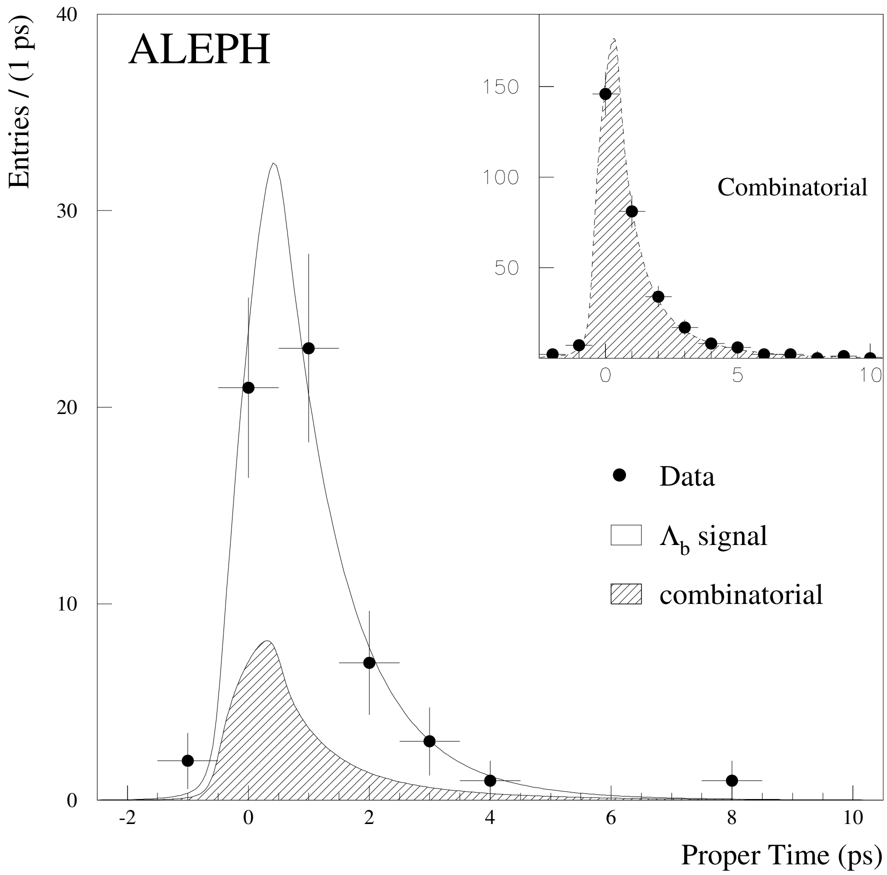

Figure 5.3: The proper-time distribution of the Λ_b candidates in the $\Lambda_c^+\ell^\perp$ sample. The shaded area corresponds to the proper-time distribution of the combinatorial background. The solid line is the result of the maximum likelihood fit described in the text.

Source	Uncertainty (ps)
Combinatorial background fraction	± 0.01
Combinatorial background shape (1/2 exponentials)	± 0.04
Physics background (1.5 ± 1.5 events)	± 0.03
Resolution function	± 0.01
Λ_{b} decay model (20% $\pm 20\%$ four-body)	± 0.02
b fragmentation	± 0.01
Λ_{b} polarization ($\mathcal{P}_{\Lambda_{\mathrm{b}}} = \perp 30^{+32}_{\perp 27}\%$)	≤ 0.01
E_{ν} calibration	≤ 0.01
Λ_{b} mass (5.6 ± 0.1) GeV/c^2	± 0.02
total	0.06

Table 5.2: Sources of systematic uncertainty in the Λ_{b} lifetime

time distribution of 58 $\Lambda_{\mathrm{c}}^{+}\ell^{\perp}$ combinations is:

$$\tau_{\Lambda_{\mathrm{b}}} = 1.02^{+0.23}_{\perp 0.18}(\mathrm{stat}) \pm 0.06(\mathrm{syst}) \text{ ps}$$

5.3 b Hadron Lifetime Measurements from all LEP Experiments

Figure 5.4 shows the current measurements of b baryon lifetime from the LEP experiments [44]. It can be seen that they are consistent with each other and the averaged b baryon lifetime is significantly smaller than the b meson lifetimes.

A summary of current b hadron lifetime measurements [44] is given in Figure 5.5. The b hadron lifetime ratios, in comparison with B^0 lifetime is shown in Figure 5.6 [44].

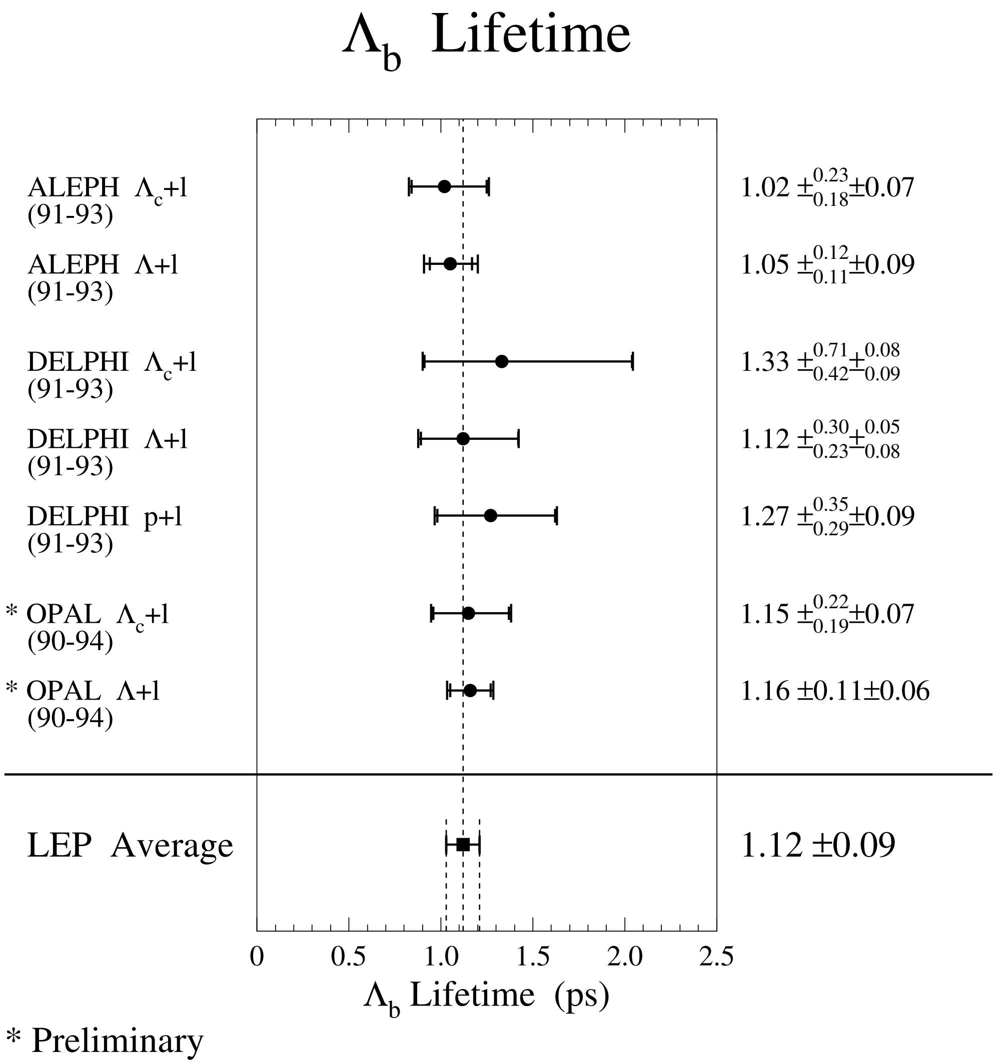

Figure 5.4: LEP measurements of b baryon lifetime.

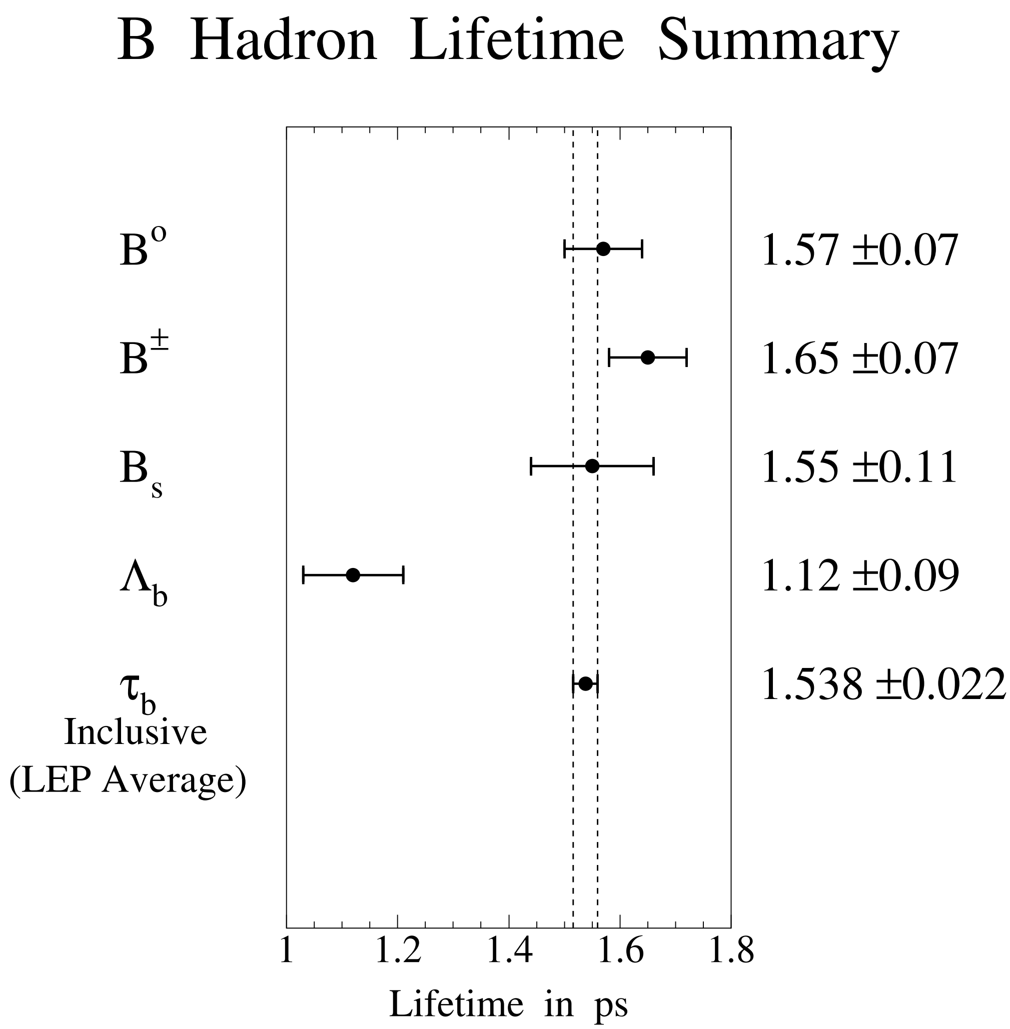

Figure 5.5: Summary of b hadron lifetime at LEP experiments.

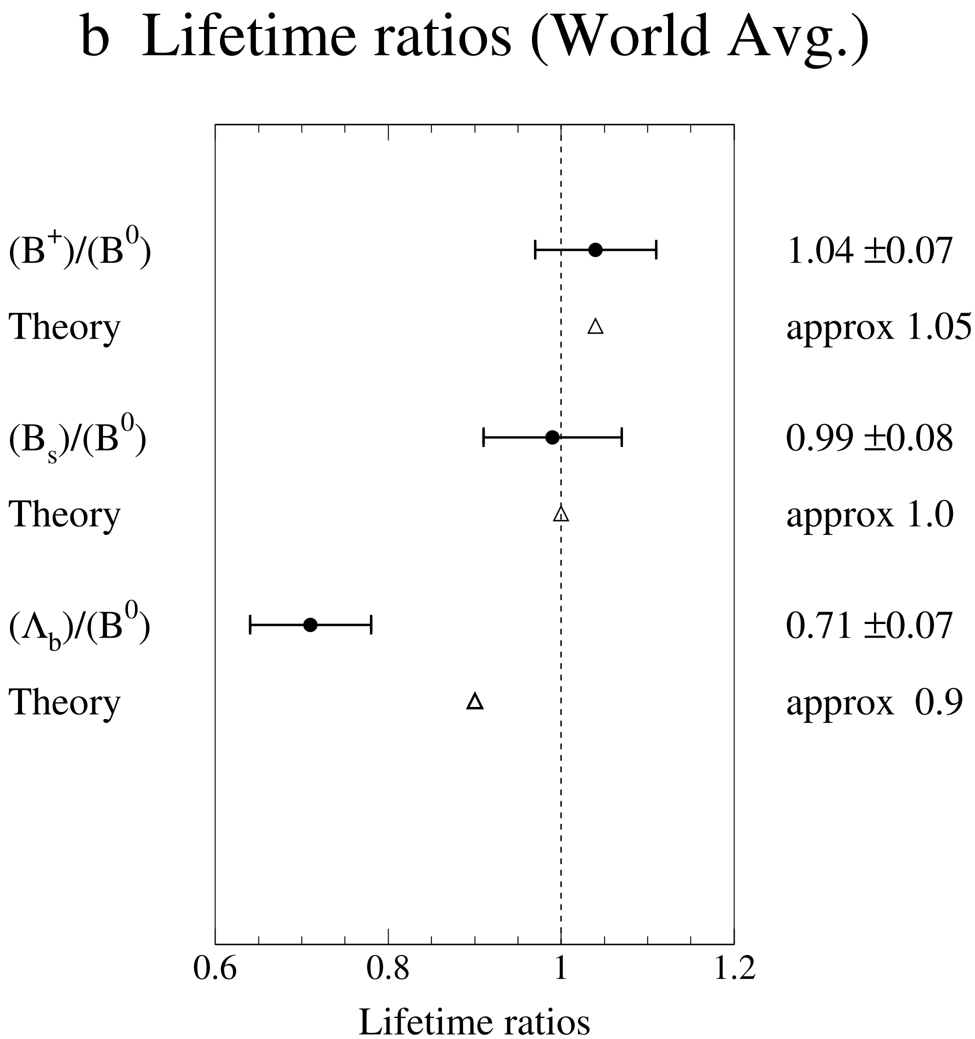

Figure 5.6: b hadron lifetime ratios (comparing with B^0).

5.4 Future Outlook

Approximately 3.0 million hadronic Z decays have been recorded with the ALEPH detector, with the end of 1994 data taking period. This means the b baryon sample identified using $\Lambda l^{\perp}$ correlation will be doubled. This will reduce the relative statistical uncertainty from the present 11% to about 8%.

Improvements to the method described in this dissertation can also be made. b baryon lifetime was measured using the 2-dimensional impact parameter of the lepton in the b baryon sample. Using 3-dimensional impact parameter will give a slightly better (about 10%) lifetime measurement with the same data sample. However, to make sure the impact parameter of lepton tracks are well measured in 3 dimensions, the lepton tracks are required to have hits in both VDET layers. Due to the geometry of the silicon microvertex detector, this requirement will reduce the lepton sample by about 15% comparing with the requirement of lepton having 1 VDET hit in the 2-dimensional impact parameter measurement. The systematic studies of 3-dimensional impact parameter measurement is similar to the 2-dimensional measurement, while obtaining the 3-dimensional impact parameter resolution from data is a bit more complicated than the 2-dimensional case. In summary, measuring b baryon lifetime using 3-dimensional impact parameter of the lepton in $\Lambda l^{\perp}$ sample will give a negligibly better measurement measurement with 1991 to 1993 ALEPH data, but 3-dimensional impact parameter method is more favored when the data sample is larger, for instance, when 1994 and 1995 data is available.

The largest systematic error in the present measurement described in this dissertation is from the uncertainty in the b baryon fraction ((58 $\pm$ 10)%) and background lepton fractions (see Table 4.2). These uncertainties are dominated by the error in the estimate of the number of accidental combinations of $\Lambda\ell^{\perp}$ with respect to $\Lambda\ell^{+}$ and the lack of the knowledge of the momentum spectra of the Λ baryons produced in the process of b or $\bar{\mathrm{b}}$ quark fragmentation. The ratio of $\Lambda\ell^{\perp}$ to $\Lambda\ell^{+}$ accidental combinations is estimated from the JETSET 7.3 simulation program as 0.8 ± 0.2. The error reflects an uncertainty in the knowledge of the momentum spectra of the Λ baryons produced in the process of b or $\bar{\mathrm{b}}$ quark fragmentation. Measuring this ratio more accurately from data is a challenge. From about 1.5 million hadronic Z decays collected with ALEPH detector between 1991 to 1993, we obtain 217 ± 24 $\Lambda\ell^{+}$ combinations where the leptons are mainly from b meson decays while the Λ's are from fragmentation. Using the b hadron semileptonic branching ratio and lepton identification efficiency, the total number of “wrong-sign" fragmentation Λ's (momentum greater than 3 GeV/c and can be reconstructed in the ALEPH detector) associated with b mesons (B^{+} or $\bar{\mathrm{B}}^{0}$ in the case of Λ, and $\mathrm{B}^{\perp}$ or B^{0} in the case of $\bar{\Lambda}$) in all 1991 to 1994 ALEPH data is about 5000. Similar number is expected for “right-sign" fragmentation Λ's associated with b mesons (B^{+} or $\bar{\mathrm{B}}^{0}$ in the case of $\bar{\Lambda}$, and $\mathrm{B}^{\perp}$ or B^{0} in the case of Λ). Considering the large number of Λ's coming from b baryon decays (about 10000 Λ's from b baryon decays, after considering all the branching ratios and reconstruction efficiency, to be compared with the 5000 “right-sign" or “wrong-sign" fragmentation Λ's associated with b hadron), it is not an easy job to get rid of the Λ's from b baryon decays while keeping enough both “right-sign" and “wrong-sign" fragmentation Λ's, and measure its ratio accurately. This can be done by identifying b meson or suppressing the presence of b baryon on one side of the event while requiring a Λ presents on the same side of the event and measure the momentum spectrum of the Λ. This will almost guarantee the Λ found on the same side of the event to be coming from fragmentation. With all the 1991 to 1994 ALEPH data, obtaining a better understanding of fragmentation Λ (both “right-sign" and “wrong-sign") momentum spectra and measuring the $\Lambda\ell^{\perp}$ to $\Lambda\ell^{+}$ ratio to a precision of better than the value of 25% used in this dissertation are feasible.

With all the 1991 to 1994 ALEPH data, the b baryon sample identified using $\Lambda_c^+\ell^{\perp}$ correlation will also be doubled. The relative statistical uncertainty of the current b baryon lifetime measurement in ALEPH using $\Lambda_c^+\ell^{\perp}$ correlation is expected to be reduced to about 15% when 1994 data is included. In this method, the Λ_c^+ candidates are reconstructed in three decay modes: $\Lambda_c^+ \rightarrow pK^{\perp}\pi^+$, $\Lambda_c^+ \rightarrow \Lambda\pi^+\pi^+\pi^{\perp}$ and $\Lambda_c^+ \rightarrow p\bar{K}^0$. With 1994 data, more decay modes ($\Lambda_c^+ \rightarrow \Lambda\pi^+$, for example) can be reconstructed. However, we do not expect a large increase in the $\Lambda_c^+\ell^{\perp}$ sample when adding these extra Λ_c^+ decay modes, due to the smallness of the branching ratio.

Bibliography

[1] Herb, S.W. et al., Phys. Rev. Lett. **39** (1977) 252;
Innes, W.R., et al., Phys. Rev. Lett. **39** 1240(1977) 1240.

[2] E. Fernandex et al., (MAC Collab.), Phys. Rev. Lett. **51** (1983) 1022;
N.S. Lockyer et al., (MARK II Collab.), Phys. Rev. Lett. **51** (1983) 1316;
W. Bartel et al., (JADE Collab.), Phys. Lett. **B114** (1982) 71.

[3] M.Kobayashi and T.Maskawa, Prog. Theor. Phys. **49** (1973) 652.

[4] M.K. Gaillard, B.W. Lee, J.L. Rosner, Rev. Mod. Phys. **47** (1975), 277;
J. Ellis, M.K. Gaillard, D.V. Nanopoulos, Nucl. Phys. **B100** (1975), 313;
J. Ellis, M.K. Gaillard, D.V. Nanopoulos, S. Rudaz, Nucl. Phys. **B131** (1977), 285.

[5] Particle Data Group, Phys. Rev. **D50** (1994).

[6] I. Bigi, "On Charm Decays - Present Status and Future Goals", SLAC-PUB-4349, 1987.

[7] I. Bigi et al., “Non-leptonic Decays of Beauty Hadrons - From Phenomenology to Theory" (in “B decays", second edition, published by World Scientific, Singapore)

[8] D. Buskulic et al., (ALEPH Collab.), Phys. Lett. **B307** (1993) 194; Phys. Lett. **B322** (1994) 275;
P. Abreu et al., (DELPHI Collab.), Z. Phys. **C57** (1993) 181; Phys. Lett. **B312** (1993) 253; Z. Phys. **C61** (1994) 407;
P.D. Acton et al., (OPAL Collab.), Phys. Lett. **B307** (1993) 247; Phys. Lett. **B312** (1993) 501; CERN-PPE/95-19; CERN-PPE/95-20.

[9] F. Abe et al., (CDF Collab.), Phys. Rev. Lett. **72** (1994) 3456.

[10] D. Buskulic et al., (ALEPH Collab.), Phys. Lett. **B297** (1992) 449;
P. Abreu et al., (DELPHI Collab.), Phys. Lett. **B311** (1993) 379;
P.D. Acton et al., (OPAL Collab.), Phys. Lett. **B316** (1993) 435.

[11] S.L. Glashow. Nucl. Phys. **22** (1961) 579;
A. Salam and J. C. Ward, Phys. Lett. **13** (1964) 168;
S. Weinberg. Phys. Rev. Lett. **19** (1967) 1264.

[12] P.W. Higgs. Phys. Lett. **12** (1964) 132;
P.W. Higgs. Phys. Rev. Lett. **13** (1964) 508;
P.W. Higgs. Phys. Rev. Lett. **145** (1966) 1156;
F. Englert and R. Brout, Phys. Rev. Lett. **13** (1964) 321.

[13] J.J. Aubert et al., Phys. Rev. Lett. **33** (1974) 1404;
J.E. Augustin et al., Phys. Lett. Lett. **33** (1974) 1406.

[14] G. Arnison et al., (UA1 Collab.), Phys. Lett. **B122** (1983) 103;
M. Banner et al., (UA2 Collab.), Phys. Lett. **B122** (1983) 476.

[15] G. Arnison et al., (UA1 Collab.), Phys. Lett. **B126** (1983) 398.

[16] ALEPH, DELPHI, L3, OPAL Collab. and the LEP Electroweak Working Group, "A Combination of Preliminary LEP Electroweak Results for the 1995 Winter Conferences", LEPEWWG/95-01.

[17] B. Andersson, G. Gustafson, G. Ingelman, T. Sjöstrand, Phys. Rep. **97** (1983) 31.

[18] C.Perterson et al., Phys. Rev. **D 27** (1983) 105.

[19] G. Altarelli, S. Petrarca, Phys. Lett. **B261** (1991) 27.

[20] I. Bigi and N.G. Uraltsev, Phys. Lett. **B280** (1992) 271.

[21] D. Decamp et al., (ALEPH Collab.), Phys. Lett. **B278** (1992), 209.

[22] P.D. Acton et al., (OPAL Collab.), Phys. Lett. **B281** (1992), 394.

[23] P. Abreu et al., (DELPHI Collab.), Phys. Lett. **B311** (1993), 379.

[24] A. Martin and J.M. Richard, Phys. Lett. **B185** (1987), 426.

[25] W. Kwong and J. Rosner, Phys. Rev. **D44** (1991) 212.

[26] D. Buskulic et al., (ALEPH Collab.), Phys. Lett. **B294** (1992) 145.

[27] D. Buskulic et al., (ALEPH Collab.), “Λ_b Lifetime Measurement", Contribution to the 27th International Conference on High Energy Physics, Glasgow, Scotland, 20-27 July 1994.

[28] “LEP Design Report", Preprint CERN-LEP/84-01, CERN, 1984.

[29] D. Decamp et al., (ALEPH Collab.), Nucl. Inst. Meth. **A294** (1990) 121.

[30] D. Buskulic et al., (ALEPH Collab.), CERN-PPE/94-170.

[31] R. Frühwirth, “Application of Filter Methods to the Reconstruction of Tracks and Vertices in Events of Experimental High Energy Physics", Preprint HEPHY-PUB 516/88, vienna, 1988.

[32] D. Buskulic et al., (ALEPH Collab.), Phys. Lett. **B313** (1993) 535.

[33] G. Lutz, Nucl. Inst. Meth. **A 337** (1993) 66.

[34] D. Buskulic et al., (ALEPH Collab.), Z. Phys. **C62** (1994) 179.

[35] J.R. Pater, “Evidence for b Baryons and B_s Mesons in Z Decays", Ph.D. dissertation, University of Wisconsin-Madison, 1993.

[36] H. Albrecht et al., (ARGUS Collab.), Phys. Lett. **B249** (1990), 359.

[37] O. Hayes, “Estimation of b Hadron Fractions in $Z \rightarrow b\overline{b}$ events", ALEPH internal report (ALEPH 94-194, PHYSICS 94-167).

[38] D. Buskulic et al., (ALEPH Collab.), “Measurement of the Λ_b polarization at LEP", Contribution to the 27th International Conference on High Energy Physics, Glasgow, Scotland, 20-27 July 1994.

[39] W. Bartel et al., Z. Phys. **C33** (1986) 23.

[40] D. Buskulic et al., (ALEPH Collab.), Phys. Lett. **B313** (1993), 535.

[41] J.H. Kühn, A. Reiter and P.M. Zerwas, Nucl. Phys. **B272** (1986) 560;

[42] D. Buskulic et al., (ALEPH Collab.), Z. Phys. **C62** (1994) 179.

[43] D. Buskulic et al., (ALEPH Collab.), Z. Phys. **C64** (1994) 361.

[44] Sau-Lan Wu, talk on “B hadron lifetimes” at the American Physical Society meeting, Washington D.C., April 1995.